

THE STELLAR MEMBERSHIP OF THE TAURUS STAR-FORMING REGION¹

K. L. LUHMAN^{2,3}

Draft version November 6, 2018

ABSTRACT

The high-precision astrometry from the second data release of the *Gaia* mission has made it possible to greatly improve the census of members of nearby clusters and associations. I have applied the *Gaia* data to the Taurus star-forming region, refining the sample of known members and identifying candidates for undiscovered members. The resulting samples of members and candidates provide the best constraints to date on the distribution of ages and the initial mass function (IMF) in Taurus. Several studies over the last 30 years have proposed the existence of a population of older stars ($\gtrsim 10$ Myr) that is associated with the Taurus clouds. The data from *Gaia* demonstrate that such a population does not exist. Meanwhile, previous IMF estimates for small fields surrounding the Taurus aggregates have exhibited a surplus of K7–M0 stars ($0.7\text{--}0.8 M_{\odot}$) relative to star-forming clusters like IC 348 and the Orion Nebula Cluster. However, that difference disappears when the new census of the entire region is considered, which should be complete for spectral types earlier than M6–M7 at $A_J < 1$. Thus, there is little variation in the stellar IMF across the 3–4 orders of magnitude in stellar density that are present in nearby star-forming regions. Finally, I note that the proper motions of two previously known members, KPNO 15 and 2MASS J04355209+2255039, indicate that they may have been ejected from the same location within the L1536 cloud ~ 7200 years ago.

Subject headings: astrometry — stars: formation — stars: kinematics and dynamics — stars: luminosity function, mass function — stars: pre-main sequence

1. INTRODUCTION

The Taurus star-forming region has served as one of the primary laboratories for investigating the process of star formation. This is in part due to its proximity to the Sun ($d \sim 140$ pc, Galli et al. 2018, references therein) and the relatively large size of its stellar population ($N \sim 400$, Kenyon et al. 2008). The importance of Taurus also stems from the unusually wide distribution of its young stars such that a comparison of the long crossing time of the region (10–20 Myr) to the age spread among its members places stringent constraints on theories for the formation of molecular clouds (Ballesteros-Paredes et al. 1999; Hartmann et al. 2001). Meanwhile, given its low stellar density ($1\text{--}10 \text{ pc}^{-3}$), Taurus can be used to search for a variation of the initial mass function (IMF) with star-forming conditions (Bonnell et al. 2011).

Measuring the distributions of ages and masses in Taurus requires a thorough census of its stellar population. Previous studies have searched for members of Taurus using signatures of youth (variability, emission lines, infrared (IR) excess emission, X-ray emission), proper motions, and optical and near-IR color-magnitude diagrams (Luhman et al. 2017, references therein). Those surveys have tended to be less sensitive to stars at older ages, but they have demonstrated that Taurus is unlikely to contain a large population of stars with ages of $\gtrsim 10$ Myr (Hartmann et al. 1991; Gomez et al. 1992).

Modest numbers of stars with ages from $\sim 10\text{--}100$ Myr have been found in the direction of Taurus, ranging from early-type stars (Blaauw 1956) to brown dwarfs (Luhman 2006; Slesnick et al. 2006; Esplin & Luhman 2017), some of which have been proposed to be products of the Taurus clouds (Walter et al. 1988; Neuhäuser et al. 1995; Wichmann et al. 1996; Daemgen et al. 2015; Kraus et al. 2017; Zhang et al. 2018). However, the surface densities and ages of those stars found in X-ray surveys are consistent with members of the solar neighborhood (Briceño et al. 1997) while most of the stars with precise proper motions are kinematically distinct from the younger stars associated with the clouds (Hartmann et al. 1991; Frink et al. 1997; de Zeeuw et al. 1999; Esplin & Luhman 2017). Nevertheless, well-defined constraints on the size of an older population in Taurus are not yet available.

Surveys for members of Taurus also have been used to derive estimates of the stellar IMF in the region (Briceño et al. 2002; Luhman et al. 2003a; Luhman 2004; Luhman et al. 2009). Those studies have found that the richest stellar aggregates exhibit a surplus of K7–M0 stars ($0.7\text{--}0.8 M_{\odot}$) relative to clusters with higher stellar densities like the Orion Nebula Cluster (ONC) and IC 348 (Hillenbrand 1997; Hillenbrand & Carpenter 2000; Muench et al. 2002, 2003; Luhman et al. 2003b). That surplus appears to be somewhat less pronounced when a larger area of Taurus is considered (Luhman et al. 2017). The most definitive comparison to other star-forming regions would employ the IMF for the entire cloud complex in Taurus, but a reliable measurement has not been possible because of uncertainties in the completeness of the current census.

As with a multitude of other topics, the astrometry from the *Gaia* mission (Perryman et al. 2001; de Bruijne

¹ Based on observations performed with the *Gaia* mission, the Two Micron All Sky Survey, and the United Kingdom Infrared Telescope Infrared Deep Sky Survey.

² Department of Astronomy and Astrophysics, The Pennsylvania State University, University Park, PA 16802; kluhman@astro.psu.edu

³ Center for Exoplanets and Habitable Worlds, The Pennsylvania State University, University Park, PA 16802, USA

2012) offers an opportunity for dramatic progress on obtaining a complete census of Taurus. The second data release of *Gaia* (DR2) contains an all-sky catalog of parallaxes and proper motions with errors of $\lesssim 0.7$ mas and $\lesssim 1.2$ mas yr⁻¹, respectively, for stars at $G \lesssim 20$ (Gaia Collaboration et al. 2018b), which corresponds to errors of $\lesssim 10\%$ and $\lesssim 5\%$ for members of Taurus at $\gtrsim 0.05 M_{\odot}$ that have low extinction. Thus, the *Gaia* data can be used for precise kinematic identification of undiscovered members of Taurus across the entire range of stellar masses. Since *Gaia* operates at optical wavelengths, heavily reddened members can fall below its detection limit, but it is the areas of high extinction near the clouds that have been most thoroughly searched for members in previous surveys, so most of the missing members (particularly older ones) are likely outside of the clouds where the extinction is low. In this paper, I have compiled the *Gaia* parallaxes and proper motions for the known members of Taurus adopted by Esplin & Luhman (2017), characterized the kinematics and distances of those objects, and checked that catalog for nonmembers (Section 2). The *Gaia* data are used to assess the membership of previous samples of older stars in the direction of Taurus (Section 3) and search for new members at any age (Section 4). Using the refined census of known members and the new candidates from *Gaia*, I estimate the distribution of ages and the IMF for Taurus (Section 5).

2. KINEMATICS OF KNOWN TAURUS MEMBERS

2.1. Retrieval of Data from *Gaia* DR2

All stars in DR2 from *Gaia* have single-epoch positions and photometry in a broad optical band (G , 3300–10500 Å). Most of those stars also have data in bands at 3300–6800 and 6300–10500 Å (G_{BP} and G_{RP}). Proper motions and parallaxes are available for most stars down to $G \sim 20$ and radial velocities are available primarily for stars at $G \sim 4$ –12. Additional data products from DR2 are described by Gaia Collaboration et al. (2018b).

To examine the kinematics and distances of known members of Taurus, I have considered the 427 stars that were adopted as members by Esplin & Luhman (2017). For each star, I identified the closest counterpart in *Gaia* DR2 within 1'' of its position in the 2MASS Point Source Catalog. Some members had multiple *Gaia* counterparts, all of which corresponded to the known components of binary systems. I retrieved the photometry, parallaxes, proper motions, and radial velocities for those counterparts from DR2. Multiple systems in which the components were unresolved from each other in the photometric catalogs utilized by Esplin & Luhman (2017) appeared as single entries in the list of members from that study. *Gaia* provides resolved measurements for companions in 13 of those systems, so they are now counted as separate objects. They consist of FQ Tau B, UX Tau C, FX Tau B, IRAS 04278+2253 B, GG Tau Bb, HN Tau B, CoKu Tau 3 B, GN Tau B, CIDA 9 B, RW Aur B, HBC 358 B, GZ Aur B, and BS Tau B.

Among the 440 objects from Esplin & Luhman (2017), 382, 336, and 28 stars have positions, parallaxes/proper motions, and radial velocities from DR2, respectively. One source, GG Tau Aa+Ab, has a negative parallax, which is likely due to its binarity. Its parallax and proper motion are excluded from this work. The median errors

in parallax, proper motion, and radial velocity for this sample are ~ 0.1 mas, 0.2 mas yr⁻¹, and 4 km s⁻¹, respectively. For most of these stars, the errors in parallax and proper motion are much smaller than those from previous measurements. Prior to *Gaia*, the most accurate parallaxes and proper motions in Taurus were measured with the Very Long Baseline Interferometry (VLBI), which produced errors comparable to that from *Gaia* for 16 systems⁴ (Loinard et al. 2005, 2007; Torres et al. 2007, 2009, 2012; Galli et al. 2018). The *Gaia* radial velocities in Taurus have limited value given that ground-based studies have measured more accurate velocities for a larger number of members (e.g., Hartmann et al. 1986; White & Basri 2003; Nguyen et al. 2012).

2.2. Analysis of *Gaia* Data

The positions of the members of Taurus from Esplin & Luhman (2017) are plotted with a map of extinction in Figure 1. The area covered by these stars has a diameter of more than 10° , which corresponds to >25 pc at their distances. One would expect a comparable spread in line-of-sight distances among the members. Indeed, Galli et al. (2018) has recently detected such a spread using parallaxes for 26 systems from VLBI and the first data release of *Gaia* (DR1). The kinematics of the stars may also vary noticeably across such a large region. Therefore, to characterize the *Gaia* proper motions and parallaxes of the known members, I have examined separately the stars within nine fields that were selected to cover subsections of the cloud complex. The boundaries for the fields are indicated in Figure 1.

Data for the members within the nine fields are shown in Figures 2–10. The few stars outside of those fields are plotted in Figures 11. Each figure contains four diagrams for the members within a given field: a map of the positions, extinction-corrected M_J versus spectral type, G versus parallax, and proper motion offsets relative to the values expected for the positions and parallaxes of the stars assuming the median space velocity of Taurus members (Section 2.3). The latter three diagrams show only stars that have *Gaia* parallaxes and proper motions. Those stars have been divided into four populations of members (labeled with red, blue, green, and cyan symbols) that exhibit distinct combinations of parallax and proper motion offsets and objects that are probable nonmembers based on these data (crosses), as discussed later in this section. The diagrams of M_J versus spectral type have been constructed with the extinctions, photometry, and spectral types adopted by Luhman et al. (2017) and Esplin & Luhman (2017). To facilitate comparison of the sequences in M_J versus spectral type among the fields, I have included the median sequences for Taurus and the Upper Sco association (11 Myr, Pecaution et al. 2012; Feiden 2016). The sequence for the latter is based on the members compiled by Luhman et al. (2018). Those diagrams of M_J versus spectral type exclude stars identified later in this section as having discrepant parallaxes. For stars that appear to have erroneous parallaxes because

⁴ Those systems consist of Anon 1 (V1096 Tau), V773 Tau, LkCa 3 (V1098 Tau), V410 Anon 25, V410 Tau (HD 283518), Hubble 4 (V1023 Tau), T Tau, RX J0424.8+2643 (V1201 Tau), HD 283641, XZ Tau, V807 Tau, HP Tau G2, LkHa 332/G1 (V1000 Tau), LkHa 332/G2 (V999 Tau), LkCa 19 (HD 282630), and HD 283572.

of binarity or that have parallax errors of $> 10\%$, I have adopted the median parallax of the kinematic population in their field to which they likely belong when computing the proper motion offsets. The plotted errors in the offsets include both the errors in the proper motions and the errors in the expected motions due to the parallax measurements. The expected motions are based on the median space velocity of Taurus members that is derived in Section 2.3.

I now discuss the four diagrams of data for each of the nine fields in Taurus.

2.2.1. B209 (Figure 2)

In the field containing the B209 cloud, the members form two distinct groups in parallax with median values of 7.6 and 6.3 mas (132 and 158 pc). These stars are plotted with red and blue symbols, respectively. The two groups also differ in their locations and proper motion offsets. The red population is projected against the B209 cloud and the smaller blue group is $\sim 1^\circ$ north of the cloud. The parallax errors for the three faintest stars in this field are too large for identification of their respective groups, so I have assigned them to the red population based on their locations and proper motion offsets.

A few members in this field have proper motions or parallaxes that differ significantly from those of the groups. MHO 3 is discrepant relative to both groups in these parameters. FO Tau is located near the stars in the red group but its parallax agrees better with that of the blue group. The parallax and location of 2MASS J04163911+2858491 are indicative of the blue population, but it has a discrepant proper motion relative to those stars. These three stars exhibit unusually poor astrometric fits among Taurus members based on the high values of the *Gaia* DR2 parameters `astrometric_gof_al` and `astrometric_excess_noise`, which can be caused by the presence of a poorly resolved binary. Indeed, FO Tau and MHO 3 are known to be tight binaries (White & Ghez 2001; Kraus et al. 2011). Therefore, I have ignored the parallaxes of these three stars, continued to treat them as members of Taurus, and assigned them to populations based on their locations.

2.2.2. L1495 (Figure 3)

Most of the members in the field for L1495 comprise a single group in both parallax and proper motion offset. They resemble the red population from B209 in both parameters and have a median parallax of 7.8 mas (128 pc). Two stars, RY Tau and IRAS 04158+2805, have discrepant parallaxes. The astrometric fits for these stars are poor according to `astrometric_gof_al` and `astrometric_excess_noise`, so both stars are retained as members and included in the red population. The poor fits may indicate the presence of tight binaries. Nguyen et al. (2012) identified RY Tau as a possible spectroscopic binary. IRAS 04158+2805 exhibits extended emission, which also may have affected the astrometry.

2.2.3. L1521, B213, and B215 (Figure 4)

The stars in the field encompassing L1521, B213, and B215 are clustered in parallax and proper motion offset like the two populations in B209 and L1495. The B213

and B215 filaments contain concentrations of stars from the blue and red groups, respectively, while the remaining members of the groups are intermingled in a wider distribution. The red and blue stars have median parallaxes of 7.6 and 6.2 mas (131 and 161 pc), respectively. As in B209, the faintest stars have uncertain parallaxes that are consistent with both populations, so they have been assigned to groups based on their proper motion offsets.

J1-4872 A appears outside of the boundaries of the diagram of proper motion offsets in Figure 4. It has a moderately poor astrometric fit, so that measurement could be erroneous. Its companion, which has a separation of $3''.4$, lacks a proper motion measurement from *Gaia*. I have retained the two stars as members. DF Tau has a moderately discrepant proper motion offset, which is likely due to its very poor astrometric fit.

2.2.4. L1527 (Figure 5)

The stars in L1527 have a single moderately broad distribution of parallaxes. The latter exhibit a gradient with right ascension, varying from ~ 8 to 7 mas between the western and eastern boundaries of the field, which indicates that the stars are related to the red population in the adjacent field to the west that contains L1527. That relationship is supported by the similar proper motion offsets. As a result, the stars in this field have been assigned to the red population.

The parallax of 2MASS J04380191+2519266, labeled with a cross in Figure 5, is much smaller than that of other members. It was identified as a candidate member of Taurus based on mid-IR excess emission (Rebull et al. 2010) and spectroscopically classified as late K or early M (Rebull et al. 2010; Esplin et al. 2014). The IR excess has served as the only evidence of its youth, and hence its membership. A second object has been detected at $1''$ from 2MASS J04380191+2519266 by *Gaia*, Pan-STARRS1 (Kaiser et al. 2002, 2010), and the United Kingdom Infrared Telescope Infrared Deep Sky Survey (UKIDSS, Lawrence et al. 2007). It is fainter by ~ 2 mag in those data and is unresolved in the images from the *Spitzer Space Telescope* that exhibited the mid-IR excess emission. As discussed earlier, close pairs of objects can have erroneous astrometry. However, the *Gaia* DR2 parameters `astrometric_gof_al` and `astrometric_excess_noise` indicate a good astrometric fit, so the parallax should be reliable. Therefore, it seems likely that 2MASS J04380191+2519266 is a field star and the mid-IR excess arises from its neighbor (perhaps a red galaxy).

V955 Tau, 2MASS J04401447+2729112, and 2MASS J04354526+2737130 have discrepant proper motion offsets, as shown in Figure 5. V955 Tau is a close binary (Leinert et al. 1993) and has a poor astrometric fit, so its proper motion is probably unreliable. The other two stars are not known binaries and have astrometric fits that are comparable to those of most other members. They are the northernmost stars in this field, and thus are farthest from other members. They could be non-members, but given their fairly large astrometric errors, they are retained as members for this study.

2.2.5. L1524, L1529, and L1536 (Figure 6)

The field with L1524, L1529, and L1536 has two populations that are similar to the red and blue groups from previously discussed clouds. Most of the red and blue stars in this field are projected against L1524/L1529 and L1536, respectively. They have median parallaxes of 7.8 and 6.2 mas (128 and 161 pc).

2MASS J04362151+2351165 and 2MASS J04344586+2445145 (crosses in Figure 6) differ from other members in their parallaxes and proper motion offsets. They are not known binaries and do not have unusually poor astrometric fits relative to other Taurus members, so there is no basis for disregarding those measurements. In addition, although the IR spectrum of 2MASS J04344586+2445145 from Luhman et al. (2017) was better matched by a young star than a field dwarf, it lacks the Li absorption expected for the former in a spectrum from the Large Sky Area Multi-Object Fiber Spectroscopic Telescope (Cui et al. 2012; Zhao et al. 2012). Both stars are treated as nonmembers in this work.

GV Tau, KPNO 15, 2MASS J04355209+2255039, and HP Tau/G2 are additional outliers in the diagram of proper motion offsets in Figure 6. The measurement for GV Tau is probably not reliable since it is a binary and it has a poor astrometric fit. The other three stars have better fits and are not known to be close binaries. All three of them reside within one of the most compact groups of stars in this field. The proper motion offsets of KPNO 15 and 2MASS J04355209+2255039 have roughly opposite directions. In fact, those data indicate that the stars were near the same location ~ 7200 years ago, as illustrated in Figure 12. Thus, KPNO 15 and 2MASS J04355209+2255039 may have been participants in a dynamical interaction with one or more additional stars (Poveda et al. 1967) that resulted in their ejection. An explanation for the discrepant motion of HP Tau/G2 is less obvious, but the VLBI motion from Galli et al. (2018) agrees better with the group, so it is retained as a member.

2.2.6. L1489 and L1498 (Figure 7)

Each of the small clouds L1489 and L1498 has a single star from Esplin & Luhman (2017) projected against it. Both stars, IRAS 04016+2610 and 2MASS 04105425+2501266, are highly reddened, so they lack *Gaia* data. Several additional young stars are scattered more widely across this field, which is west of the main complex of clouds in Taurus. Two and four of those stars have similar parallaxes and proper motions as the red and blue populations from the main cloud complex, respectively. The two remaining systems in this field are HBC 358 ABC and HBC 359, which have a separation of $20''$. HBC 358 A and BC are separated by $1''.6$ and HBC 358 B and C are separated by $0''.15$ (Hartigan & Kenyon 2003). Parallaxes and proper motions from *Gaia* are available for HBC 358 BC and HBC 359, which are labeled with crosses in Figure 7⁵. Their proper motion offsets differ from those of the populations associated with Taurus clouds, so all members of these systems are classified as nonmembers.

⁵ Near-IR photometry is not available for HBC 358 BC, so it does not appear in the diagram of M_J versus spectral type in Figure 7.

2.2.7. L1551 and L1558 (Figure 8)

The southernmost clouds in Taurus include L1558, L1551, the small cloud near T Tau, and cloud 18 from Onishi et al. (2002), which contains the protostars IRAS 04191+1523 and IRAM 04191+1522. Most of the young stars in the field encompassing these clouds form a well-defined group that resembles the blue populations from the northern clouds except with slightly larger parallaxes and smaller proper motion offsets in declination. The median parallax for that group is 6.9 mas (145 pc). The two stars near T Tau are similar to that population in parallax but differ in their proper motion offsets. The latter are closer to the values of the red populations in the previous fields, so the same color is assigned to them. In proper motion, T Tau agrees better with the blue group than its two neighbors, so it is unclear to which population it belongs. I have assigned it to the same group as its neighbors. The five stars near L1558 have parallaxes and proper motion offsets that are distinct from those of the red and blue groups, so they are labeled with a third color of green. They have a median parallax of 5.1 mas (196 pc), making them the most distant members of Taurus.

Some of the young stars in this field are outliers in parallax and proper motion relative to the red, blue, and green groups. HD 30171 is similar to the blue stars in terms of its proper motion offset and is located $13''$ from a member of the blue group, IRAS 04429+1550. Its parallax from DR2 is too small for that group (5.41 ± 0.11 mas), but its measurement from DR1 is in better agreement (7.07 ± 0.24 mas). Therefore, I have assigned it to the blue population. A second star with a discrepant parallax is LkHa 358. It has a moderately poor astrometric fit relative to other members of Taurus, which is probably due to the presence of extended emission surrounding this protostar. I have ignored the *Gaia* measurement of its parallax and have retained it as a member. Haro 6-37 A is one of the stars near L1558 labeled in green. Its parallax differs from that of the other green stars, but the parallax of its companion Haro 6-37 B does agree with that group, so both stars are considered members of it. Finally, J2-157 and 2MASS J04284199+1533535 (crosses in Figure 8) differ from the groups in this field in both their parallaxes and proper motion offsets. The quality of the astrometric fit for each star is comparable to that of the fits for most Taurus members, so those measurements should be reliable. They are excluded from my catalog of members.

2.2.8. L1517 (Figure 9)

Most of the young stars in the field for L1517 are members of a single group in parallax and proper motion offset. The median parallax for this group is 6.3 mas (159 pc). Some stars are clustered around L1517 while others are more widely distributed. The distributions of parallax and proper motion offsets overlap with those of the red and blue groups from other clouds, but they are sufficiently distinct that I have labeled them with a fourth color of cyan.

2MASS J04485789+2913548, Haro 6-39, 2MASS J04555288+3006523, and 2MASS J04591661+2840468 do not match the population in this field in terms of either parallax or proper motion offset. The first two stars

have poor astrometric fits and the first is $6''$ from a member of the cyan group (2MASS J04485745+2913521), so I ignore their astrometry and treat them as members of that group. 2MASS J04555288+3006523 and 2MASS J04591661+2840468 have better astrometric fits, so they are likely to be nonmembers. They are labeled with crosses in Figure 9. 2MASS J04555288+3006523 is beyond the boundaries of the diagrams of parallax and proper motion offset. 2MASS J04591661+2840468 does not appear in the diagram of M_J versus spectral type since it lacks a spectral classification.

2.2.9. L1544 (Figure 10)

A single group in parallax and proper motion offset is present among the stars in the L1544 field. It overlaps with the cyan population in L1517 in those parameters, so it has been assigned that color. The median parallax is 5.8 mas (172 pc).

2MASS J05122759+2253492 and CIDA 11 are discrepant in their parallax and proper motion, respectively. Both stars have poor astrometric fits, so they are retained as members. They have been resolved as close pairs by *Gaia* and Kraus et al. (2011), respectively, which would explain the poor fits. 2MASS J05023985+2459337 also does not match the proper motion offset of the group in this field. It does agree better with the motions of the southernmost stars in the field for L1517, so it could be a member of that population. The astrometric fit appears to be reliable. It is unclear whether this star should be treated as a member of Taurus, but I do so for the purposes of this work.

2.2.10. Stars Outside of Previous Fields (Figure 11)

Twelve stars from the catalog of members adopted by Esplin & Luhman (2017) are outside of the fields in Figures 2–10. All but one have measurements of parallaxes and proper motions from *Gaia* DR2. Eight of those 11 stars differ significantly from the populations associated with the Taurus clouds in terms of their parallaxes and proper motion offsets (crosses in Figure 11). They consist of HBC 360, HBC 361, HBC 362, 2MASS J04102834+2051507, 2MASS J04110570+2216313, 2MASS J04162725+20530, 2MASS J04345973+2807017, and 2MASS J05064662+2104296. The astrometric fits for the HBC 360 and HBC 361 are moderately poor while the other stars have better fits. Those two stars have a separation of $7''$ and are $14'$ from HBC 362. The three stars share similar proper motions and parallaxes, which suggests that those measurements are reliable (and that the stars are associated with each other). These eight stars are rejected from my catalog of members.

The remaining three stars with *Gaia* data are 2MASS J04225416+2439538, CoKu Tau 4, and CIDA 14. The astrometry for 2MASS J04225416+2439538 agrees well with that of the red populations in the clouds that are closest to it. CoKu Tau 4 is a known binary with a separation of $0''.05$ (Ireland & Kraus 2008), but its astrometric fit is not especially poor, so its astrometry is probably reliable. Both CoKu Tau 4 and CIDA 14 are north of L1527 and southwest of L1517 and they have similar parallaxes and proper motion offsets. In those parameters, the two stars are near the clusters of values for the red and cyan populations in those clouds,

although they do not overlap with either group in both parameters simultaneously. They agree slightly better with the cyan population in L1517, so they have been assigned that color for the purposes of the figures.

HD 286178 is the one star from Esplin & Luhman (2017) outside of the fields in Figures 2–10 that lacks a parallax and proper motion from *Gaia*. Those parameters were not measured because the astrometric fit was very poor. Given its remote location relative to the Taurus clouds and the presence of young stars across Taurus that are kinematically unrelated to the clouds (Sections 1 and 3), it seems likely that HD 286178 is a nonmember, so I treat it as such.

2.3. Revised Catalog of Members

As discussed in the previous section, I have rejected 19 of the 440 stars adopted as Taurus members by Esplin & Luhman (2017). For reasons described in Sections 3 and 4, I also have assigned membership to 17 additional stars, consisting of HD 28354, HD 283641, HD 283782, HD 30378, RX J0422.1+1934, L1551-55, RX J0507.2+2437, JH 223 B, XEST 20-071 B, V892 Tau NE, 2MASS J04284263+2714039 B, 2MASS J05080816+2427150 B, PSO J065.8871+19.8386, PSO J071.6033+17.0281, PSO J071.3189+31.6888, PSO J074.1999+29.2197, and PSO J076.2495+31.7503. The revised catalog of 438 Taurus members is presented in Table 1.

In Table 1, I have included the proper motions and parallaxes from *Gaia* DR2, radial velocities from previous studies, *UVW* space velocities computed from the *Gaia* data and radial velocities (Johnson & Soderblom 1987), the three bands of *Gaia* photometry, and the color codes for the kinematic populations described in the previous section. A few of the radial velocity measurements lack estimates of errors. In those cases, an error of 1 km s^{-1} has been adopted when calculating the *UVW* errors. I have not used the radial velocity measurement for HN Tau A from Nguyen et al. (2012) because its systematic noise is large. Systematic errors in the *Gaia* DR2 parallaxes are expected to be less than 0.1 mas (Gaia Collaboration et al. 2018b). Recent studies have found that those parallaxes may be too small by ~ 0.08 mas on average (Kounkel et al. 2018; Stassun & Torres 2018). Since such errors may vary with position on the sky and their average value in the direction of Taurus is unknown, no correction has been applied to the parallaxes when deriving *UVW* velocities. The latter have not been computed for stars that have discrepant parallaxes based on the analysis in the previous section. Table 1 contains estimates of *UVW* for 100 stars. The median of those velocities is $U, V, W = -15.9, -12.4, -9.4 \text{ km s}^{-1}$, which is similar to values from Bertout & Genova (2006) and Luhman et al. (2009). That median *UVW* was used in the calculation of the proper motion offsets in Figures 2–11.

In Table 2, I have compiled the medians of the parallaxes, proper motions, and proper motion offsets and the standard deviations of the proper motions for each of the fields and populations in Figures 2–10. Only stars with parallax errors of $\leq 10\%$ and non-discrepant parallaxes have been considered. If standard deviations are calculated for proper motions with errors of $< 0.25 \text{ mas yr}^{-1}$, the most compact aggregates (those

in B209, L1495, L1529, L1536, L1551, L1517) have one-dimensional dispersions of $\sim 1 \text{ mas yr}^{-1}$, which corresponds to $\sim 0.7 \text{ km s}^{-1}$ at the distances of the stars. Since these values are significantly larger than the proper motion errors, they should be dominated by the kinematics within the aggregates.

For groups of 3 or more stars that are near clouds and that have measurements of UVW , I have calculated the medians of the parallaxes, proper motions, and UVW and the standard deviations of UVW . The results are listed in Table 3 with their associated clouds. The dispersions are larger in U than V and W because the radial velocities generally have larger errors than the proper motions. In Figure 13, I have plotted the corresponding XYZ positions in Galactic Cartesian coordinates and the median UVW 's relative to the median value for Taurus. The five aggregates labeled as red have similar velocities, which is not surprising given their proper motion offsets (Figs. 2–6). The two aggregates labeled as blue, L1536 and L1551, have similar motions and differ from the red aggregates by $\sim 3 \text{ km s}^{-1}$ in each of the V and W components. The small aggregate associated with L1558 (green) differs by $\sim 3 \text{ km s}^{-1}$ from the other groups in U and is similar to the blue and red groups in V and W , respectively. It is also the most distant aggregate in Taurus at nearly 200 pc, as mentioned in Section 2.2.7. The cyan group near L1517 is similar to the blue/green and red groups in V and W , respectively. The total spread among the aggregates is $\sim 3 \text{ km s}^{-1}$ in each of the velocity components. Those relative motions correspond to $\sim 3 \text{ pc}$ ($\sim 1^\circ$) in 1 Myr, or $\sim 10\%$ of the diameter of the cloud complex, as illustrated in Figure 13.

3. PREVIOUS CANDIDATE MEMBERS AT OLDER AGES

Several studies over the last 30 years have proposed the existence of stars with ages of $\gtrsim 10 \text{ Myr}$ that are associated with the Taurus clouds (Section 1). In this section, I use astrometry from *Gaia* DR2 to assess the membership of such stars from Kraus et al. (2017) and Zhang et al. (2018).

3.1. Candidates from Kraus et al. (2017)

Kraus et al. (2017) compiled a catalog of 396 diskless stars that had been previously identified as possible members of Taurus. Through analysis of several diagnostics (e.g., proper motions, radial velocities, spectroscopic signatures of youth), they concluded that 218 of the candidates were confirmed or likely members. Roughly 1/3 of those suggested members were absent from earlier compilations, most of which were older ($\gtrsim 10 \text{ Myr}$) and more widely distributed than the canonical members. Kraus et al. (2017) proposed that these stars represent an earlier generation of star formation associated with the Taurus cloud complex.

Among the 218 stars that Kraus et al. (2017) designated as members, 82 were absent from the census in Luhman et al. (2017). Esplin & Luhman (2017) examined the astrometric evidence of membership for those 82 stars. Sixteen of them had measurements of parallaxes and proper motions from *Gaia* DR1 and appeared between $\alpha = 4^{\text{h}}-5^{\text{h}}10^{\text{m}}$ and $\delta = 15-31^\circ$, which corresponds roughly to the boundaries of Figure 1 and encompasses all of the Taurus clouds. Esplin & Luhman (2017) compared the proper motions, parallaxes, and M_J for

those stars and members from Luhman et al. (2017) that had *Gaia* DR1 data. Most of the former were kinematically distinct from the latter and exhibited older ages ($\gtrsim 10 \text{ Myr}$). The two samples differed by $\sim 10 \text{ mas yr}^{-1}$ on average, which corresponds to a relative drift of nearly 30° over 10 Myr, indicating that they are physically unrelated.

Gaia DR2 enables a comprehensive analysis of the candidate members from Kraus et al. (2017). The compilation of members from Esplin & Luhman (2017) does not contain 85 of the 218 stars identified by Kraus et al. (2017) as probable members. Fifty-two of those 85 stars are within the field defined by $\alpha = 4^{\text{h}}-5^{\text{h}}10^{\text{m}}$ and $\delta = 15-31^\circ$ and have parallaxes from *Gaia* DR2 with errors of $\leq 10\%$. They are plotted in diagrams in Figure 14 like those in Figures 2–11. Four stars have parallaxes and proper motions offsets that overlap with the populations of members in Figures 2–11, consisting of L1551-55, RX J0507.2+2437, RX J0422.1+1934, and HD 283782. The first two stars were in the census from Luhman et al. (2017) but were rejected by Esplin & Luhman (2017). I adopt these four stars as members. One star, HBC 392, is somewhat close to the distribution of parallaxes and proper motion offsets for one of the Taurus groups, L1551. It has unusually weak Li absorption for a Taurus member (Walter et al. 1988), which has been cited as evidence that it is a nonmember (Hartmann 2003) or a Li-depleted member (Sestito et al. 2008). HBC 392 appears below the median sequence for Upper Sco (11 Myr, Pecaute et al. 2012) in M_J versus spectral type, indicating that its weak Li is a reflection of an older age. Based on its *Gaia* astrometry and its radial velocity (Nguyen et al. 2012), it has a space velocity of $U, V, W = -14.4 \pm 0.1, -16.1 \pm 0.1, -9.2 \pm 0.1 \text{ km s}^{-1}$, which differs from the median velocity of L1551 (Table 3) by $\sim 1.5 \text{ km s}^{-1}$ in each component. That difference corresponds to a relative drift of $>20 \text{ pc}$ ($> 9^\circ$) on the plane of the sky since the star was born, assuming an age of $> 10 \text{ Myr}$. Thus, it is unlikely that HBC 392 originated in that cloud, and it is not adopted as a Taurus member in this work.

Hartmann et al. (1991) suggested that a previous sample of $\gtrsim 10 \text{ Myr}$ stars towards Taurus from Walter et al. (1988) belong to the Cas-Tau association, whose proposed members encompass the Taurus clouds and extend well beyond them (Blaauw 1956). Therefore, I have considered that possibility for the 47 stars in Figure 14 that differ kinematically from the Taurus populations. de Zeeuw et al. (1999) identified a sample of 83 B and A stars that may be members of Cas-Tau. *Gaia* DR2 has provided parallaxes with errors of $\leq 10\%$ for 80 stars in that sample. Radial velocity measurements with errors of $< 4 \text{ km s}^{-1}$ are available for 33 of those 80 stars (de Bruijne & Eilers 2012). The radial velocities combined with the *Gaia* astrometry produce space velocities that have a median value of $U, V, W = -15.3, -22.0, -7.3 \text{ km s}^{-1}$, which is similar to the values derived prior to *Gaia* DR2 (de Zeeuw et al. 1999; David et al. 2018). The median velocity of Cas-Tau differs significantly from that of Taurus ($U, V, W = -15.9, -12.4, -9.4 \text{ km s}^{-1}$), as noted by de Zeeuw et al. (1999). The 80 proposed Cas-Tau members from de Zeeuw et al. (1999) that have *Gaia* data

are included in the bottom diagrams in Figure 14. Their parallaxes and proper motion offsets overlap with those of roughly half of the 47 stars from Kraus et al. (2017) that are kinematically distinct from Taurus. Thus, it is plausible that the latter are members of Cas-Tau.

Most of the remaining stars in Figure 14 that do not overlap with Cas-Tau form a clump in parallax and proper motion offset that is centered near 8.25 mas and $(-8.2, 7.0 \text{ mas yr}^{-1})$, respectively. This clump coincides with group 29 from Oh et al. (2017), which is a possible new association of nine stars found with *Gaia* DR1. Several of the stars from the catalog of members in Esplin & Luhman (2017) that were rejected in Section 2.2 also appear in that clump (see Figs. 6, 8, 11). To investigate the nature of this group, I selected stars from *Gaia* DR2 that are within 0.35 mas and 2 mas yr^{-1} of the clump’s center, which are the values beyond which the number of stars rapidly decreases. All of the nine stars identified by Oh et al. (2017) as members of group 29 satisfy that proper motion threshold, but four of them fall outside of the parallax threshold. To allow for the possibility that members of the group might extend beyond the confines of Taurus, I considered the area between $\alpha = 3^{\text{h}}-6^{\text{h}}$ and $\delta = 4-40^{\circ}$. Most of the stars in the resulting sample (91/107) are within the boundary of the map of Taurus in Figure 14, so the following discussion is restricted to those stars. Their spatial distribution is shown in the map in Figure 15. Measurements of radial velocities are available for 23 of the 91 stars (Walter et al. 1988; Nguyen et al. 2012; Kraus et al. 2017, *Gaia* DR2). The velocities have a dispersion of $\sim 1.4 \text{ km s}^{-1}$, which is only somewhat larger than the dispersion of velocities on the plane of the sky imposed by the selection criteria ($\sim 0.5 \text{ km s}^{-1}$). The median space velocity for those 23 stars is $U, V, W = -13.0, -6.4, -9.7 \text{ km s}^{-1}$, differing by a total of 6.6 km s^{-1} from the median motion of Taurus.

The ages of the 91 candidate members of group 29 can be estimated with a diagram of absolute magnitude versus color. Since *Gaia* photometry has very high precision, the diagram has been constructed with G_{BP} and G_{RP} , as shown in Figure 15. A comparison of those stars to members of the Pleiades (Stauffer et al. 2007) in $G_{\text{RP}} - K_s$ versus $J - H$ indicates that they have little extinction, so extinction corrections have not been applied to the photometry. In Figure 15, the stars form a sequence that is fairly narrow and well-defined, which suggests that they comprise a coeval population. To estimate the age of this sample, I have compared its sequence to those of nearby clusters and associations that span a range of ages (Bell et al. 2015; Gagné et al. 2018, references therein). In Figure 15, I have included fits to the single-star sequences for three populations that bracket the sample, consisting of the β Pic moving group (24 Myr, Bell et al. 2015), the Tuc-Hor association (45 Myr, Bell et al. 2015), and the Pleiades cluster (112 Myr, Dahm 2015). The fits are defined in Table 4. This comparison suggests that group 29 is slightly younger than Tuc-Hor ($\sim 40 \text{ Myr}$). The velocity offset of 6.6 km s^{-1} relative to the Taurus combined with an age of 40 Myr corresponds to a relative drift of 260 pc, indicating that the stars have no relationship to the gas that would eventually form the Taurus clouds. Like Cas-Tau and the Hyades, group 29

is another example of a stellar population that lies in the direction of Taurus but is unrelated to the cloud complex. Astrometry and photometry for the 91 candidate members of group 29 are presented in Table 5. Among these stars, HD 284149 and HBC 376 (TAP 26) are known to harbor a brown dwarf companion and a hot Jupiter (Bonavita et al. 2014; Yu et al. 2017), respectively.

It was not included in the sample of stars analyzed by Kraus et al. (2017), but St34 was cited in that study as an example of an old member of Taurus ($\gtrsim 20 \text{ Myr}$). White & Hillenbrand (2005) found that it is a spectroscopic binary in which the components have similar luminosities and spectral types. It appeared to reside in Taurus based on its kinematics and its evidence of youth in the form of an accretion disk, but the components lacked Li absorption, indicating an age of $> 20 \text{ Myr}$. White & Hillenbrand (2005) concluded that St34 is probably a relatively old member of Taurus ($\gtrsim 8 \text{ Myr}$). Meanwhile, Hartmann et al. (2005) proposed that the system is not associated with the Taurus clouds, and that instead it lies in the foreground at a distance of $\sim 100 \text{ pc}$, which appeared to alleviate the discrepancy between the ages inferred from the luminosity and the absence of Li absorption. According to the parallax measurement from *Gaia* DR2, St34 has a distance of $142.7 \pm 1.2 \text{ pc}$, which places it within the range of distances of Taurus members. However, the kinematics of St34 are inconsistent with membership in Taurus. Based on the astrometry from *Gaia* and the radial velocity from White & Hillenbrand (2005), the system has a space velocity of $U, V, W = -15.1 \pm 0.7, -6.9 \pm 0.1, -10.7 \pm 0.1 \text{ km s}^{-1}$, which differs by $\gtrsim 4 \text{ km s}^{-1}$ from the median motions of the groups in Taurus (Table 3). The data for St34 are included in both Figures 14 and 15. The photometry has been corrected for the binarity by assuming that the components have equal fluxes. For a single component, the spectral type and M_J relative to the median sequence of Upper Sco suggests an age of $\sim 20 \text{ Myr}$ (Baraffe et al. 2015) while the position in the color-magnitude diagram relative to the β Pic and Tuc-Hor associations indicates an age of $\sim 30 \text{ Myr}$. The latter value could be overestimated if the system has excess emission in G_{BP} from accretion. An age of 20–30 Myr is consistent with the constraints on the Li abundance (White & Hillenbrand 2005).

3.2. Candidates from Zhang et al. (2018)

Zhang et al. (2018) presented a sample of 58 late-type objects that they classified as members of Taurus. Most of them are fainter than the known members at a given color or spectral type, indicating that they are older or more distant. Zhang et al. (2018) concluded that these objects represent an older population ($\gtrsim 10 \text{ Myr}$) that is similar to the one proposed by Kraus et al. (2017).

The membership of the candidates from Zhang et al. (2018) can be assessed with data from *Gaia* DR2, which became available after that study. Among the 58 candidates, 47 have entries in *Gaia* DR2 and 38 have parallax measurements (15 with errors of $\leq 10\%$). In Figure 16, all of the candidates are plotted on a map of Taurus and a diagram of extinction-corrected J versus spectral type (Zhang et al. 2018). Those diagrams also include the stars from Esplin & Luhman (2017) that are adopted as members in this work. The stars with par-

allax measurements are shown in diagrams of G versus parallax and proper motion offsets relative to the motion expected for the median space velocity of known Taurus members. For those offsets, I have adopted the parallactic distances when the parallax errors are $\leq 10\%$ and otherwise have assumed a distance of 140 pc.

Five of the 38 candidates with *Gaia* parallaxes and proper motions overlap with the groups of known members in those parameters, consisting of PSO J065.8871+19.8386, PSO J071.3189+31.6888, PSO J071.6033+17.0281, PSO J074.1999+29.2197, and PSO J076.2495+31.7503. Based on those data and the evidence of youth in the spectra from Zhang et al. (2018), I have adopted them as members of Taurus. Three of those five objects, PSO J065.8871+19.8386, PSO J071.6033+17.0281, and PSO J074.1999+29.2197, have been independently identified as members by Esplin & Luhman (2018). Among the remaining 33 candidates with *Gaia* astrometry, PSO J070.2057+27.5378 and PSO J079.3986+26.2455 are somewhat close to the distributions of parallaxes and proper motion offsets for L1517 and L1544, respectively, but are located rather far from those clouds ($\sim 3^\circ$). Given that young stars unrelated to the Taurus clouds are scattered across this area of sky (Section 3.1), those two stars have insufficient evidence of membership. The remaining 31 candidates with *Gaia* data have discrepant parallaxes and proper motions (see Fig. 16), and thus are excluded from my catalog of members. All of the five candidates from Zhang et al. (2018) that have kinematics consistent with membership appear within the Taurus sequence in the diagram of J versus spectral type, indicating that they are within the age range of the known members. None of the candidates for older members with *Gaia* astrometry have been confirmed as such by those data.

Gaia parallaxes and proper motions are unavailable for 20 of the candidates from Zhang et al. (2018). Given the lack of astrometry with sufficient precision to distinguish between Taurus members and young contaminants, I assess those candidates with the ages implied by the color-magnitude diagram in Figure 16 and the proximity to the Taurus clouds. The use of age as a criterion is justified by a search of *Gaia* DR2 for undiscovered members at higher masses in Section 4, which demonstrates that a population older than the known members does not exist. Two of the 20 candidates that lack *Gaia* astrometry, PSO J064.6887+27.9799 and PSO J065.1792+28.1767, are within the sequence of known members in the diagram of J versus spectral type and are near the clouds. They were independently found and classified as members by Esplin & Luhman (2017). A few additional candidates like PSO J059.5714+30.6327 may be as young as the known members, but they are far from the clouds and cannot be reliably distinguished from young contaminants with the available data. Most of the 20 candidates are too faint to be members that are coeval with the known Taurus population, as shown in Figure 16.

Among the seven candidates from Zhang et al. (2018) that are included in my catalog of members, five have been spectroscopically classified by Esplin & Luhman (2017, 2018), who derived the following spectral types: M9.25 (IR) for PSO J064.6887+27.9799 and J065.1792+28.1767, M7 (op-

tical) for PSO J071.6033+17.0281, M6 (optical) for PSO J074.1999+29.2197, and M9 (optical/IR) for PSO J065.8871+19.8386. I have measured a type of M5.5 for both of the remaining two stars, PSO J071.3189+31.6888 and PSO J076.2495+31.7503, using the IR spectra from Zhang et al. (2018). For those seven stars, the classifications from Zhang et al. (2018) are later than those from Esplin & Luhman (2017, 2018) and this work by an average of ~ 1 subclass. In addition to their candidates, Zhang et al. (2018) classified IR spectra of most known late-type members of Taurus. In Figure 17, those types are compared to the optical spectral types that are available for those objects (Briceño et al. 1998, 2002; Martín & Magazzù 1999; Hartigan & Kenyon 2003; White & Basri 2003; Guieu et al. 2006; Slesnick et al. 2006; Luhman 2004, 2006; Luhman et al. 2003a, 2006, 2009; Esplin et al. 2014; Herczeg & Hillenbrand 2014)⁶. Once again, the classifications from Zhang et al. (2018) are systematically later by ~ 1 subclass. Thus, their types cannot be used alongside the previous optical types in a meaningful way. The IR types from my previous studies are based on comparison to optically-classified members of Taurus and other star-forming regions (Luhman et al. 2017), which are the ideal standards for producing IR types that are on the same system as the optical types.

4. SEARCH FOR NEW MEMBERS

The data from *Gaia* DR2 can be used to search for stars associated with the Taurus clouds with a high degree of completeness for all locations, ages, and stellar masses with the exception of the most highly reddened members. Most of the latter are likely to be younger and less evolved, and hence should have been found by mid-IR surveys for stars with circumstellar disks (Beichman et al. 1986; Kenyon et al. 1990; Luhman et al. 2006; Rebull et al. 2010; Esplin et al. 2014).

For each of the nine fields in Figure 1, I selected stars that have measurements of parallaxes from *Gaia* DR2 with errors of $\leq 10\%$ and that are within 0.5 mas and 4 mas yr⁻¹ of the median parallaxes and proper motion offsets of any of the populations of known members within that field (Table 2). These thresholds were selected to be large enough to recover most (95%) of the known members that have the necessary *Gaia* data and that do not have discrepant parallaxes (Section 2.2). If larger thresholds are adopted, only a few additional candidates coeval with the known Taurus population are selected while the number of candidates older than Taurus increases roughly in proportion to the square of the thresholds, which is consistent with a population of field contaminants. Among the candidates selected by my criteria, I have assigned membership to those with previous spectroscopic data that are consistent with membership and those that are within a few arcseconds of known members, and hence are likely to be companions. They consist of HD 28354,

⁶ Most of these optical types were derived via comparison to the average spectra of dwarf and giant standards (Henry et al. 1994; Kirkpatrick et al. 1991, 1997), which is a scheme that has been applied to M5–M9.5 members of Taurus and other star-forming regions during the past two decades (Luhman et al. 1997, 1998a,b; Luhman 1999, 2012, references therein).

HD 30378, HD 283641, JH 223 B, V892 Tau NE, XEST 20-071 B, 2MASS J04284263+2714039 B, and 2MASS J05080816+2427150 B. I rejected candidates that have been previously classified as evolved stars or that have radial velocities that differ significantly ($> 5 \text{ km s}^{-1}$) from the median velocities of the Taurus populations, which applies to all (9) candidates for which velocities have been measured. All of the candidates rejected by radial velocities are also much fainter than the known members of Taurus at a given color, which further suggests that they are field stars. After these steps, there remain 141 candidate members, which have magnitudes ranging from $G \sim 13\text{--}20$.

To estimate the ages of the candidates, I have plotted the ones with measurements of G_{BP} and G_{RP} (114 of the 141 candidates) in a diagram of $M_{G_{\text{RP}}}$ versus $G_{\text{BP}} - G_{\text{RP}}$ in Figure 18. As done in Figure 15, I have included fits to the single-star sequences for the β Pic and Tuc-Hor associations and the Pleiades cluster. In an optical color-magnitude diagram, stars with disks occasionally appear below the sequence for their population if their observed flux is dominated by scattered light or if accreting material generates bright excess emission at shorter wavelengths. Therefore, to more clearly define the sequence for Taurus in Figure 18, only members that lack disks are shown (Esplin et al. 2014; Esplin & Luhman 2017). Members with discrepant parallaxes are excluded (Section 2.2).

Many members of Taurus have substantial extinction, which affects their locations in a color-magnitude diagram. Because the *Gaia* photometric bands are quite broad, the relation between the extinction in a given band and the extinction at a specific wavelength depends noticeably on the amount of extinction and the intrinsic spectrum (or color) of the object (Gaia Collaboration et al. 2018a; Danielski et al. 2018). A reddening vector that is applicable to typical members of Taurus is shown in Figure 18. Since the vector is largely parallel to the Taurus sequence, the variable extinction among the members should not broaden the sequence significantly. Meanwhile, most of the candidate members closely match the sequence of Pleiades members (Stauffer et al. 2007) in color-color diagrams like $G_{\text{RP}} - K_s$ versus $J - H$, indicating that they have little extinction. For these reasons, I have not attempted to correct the data in Figure 18 for extinction.

The candidates exhibit two distinct distributions in Figure 18, one that is scattered within the sequence of known Taurus members and another that appears below the Tuc-Hor sequence ($\gtrsim 40 \text{ Myr}$). None of the latter show evidence of disks in mid-IR photometry from the *Spitzer Space Telescope* (Werner et al. 2004) or the *Wide-field Infrared Survey Explorer* (Wright et al. 2010), so their low positions in the diagram are not attributable to scattered light. The sharp decrease in the number of members and candidates below the lower envelope of the Taurus sequence indicates that there are few, if any, stars at ages of 10–40 Myr that are associated with the Taurus clouds. Given the paucity of candidates in that age range, it is highly unlikely that the stars at $>40 \text{ Myr}$ have any relationship to Taurus. Indeed, most of the older candidates appear near the selection thresholds for parallax and proper motion offsets or have larger astrometric errors, whereas the younger candidates are more

tightly clustered with the known members in those parameters. In addition, the matching population for more than half of the older candidates was L1558, which contains only five known members. The unrealistically large number of candidates is likely a reflection of the fact that this group is the most distant one in Taurus ($\sim 200 \text{ pc}$) and the number of stars satisfying the proper motion criteria increases rapidly with larger distances. To verify the plausibility that the older candidates comprise unrelated contaminants, I performed multiple iterations of the selection of candidates with uniform shifts applied to the median proper motion offsets of the Taurus groups (e.g., $\pm 10 \text{ mas yr}^{-1}$). The resulting samples of stars closely resemble the older candidates selected for Taurus in size and distribution of colors and absolute magnitudes.

In Table 6, I present the 54 candidates that have estimated ages of $\lesssim 20 \text{ Myr}$. They consist of the 49 stars in Figure 18 that appear above the sequence for β Pic, three candidates that have photometry in only one band (G) but that are candidate companions to stars that are bright enough to appear in the Taurus sequence, and two candidates that lack G_{BP} but are young according to a diagram of $M_{G_{\text{RP}}}$ versus $G - G_{\text{RP}}$. Spectroscopy of the candidates is necessary to measure their spectral types and verify their youth. Esplin & Luhman (2018) has classified spectra of many of the candidates, all of which show evidence of youth that is consistent with the ages inferred from Figure 18. Most of those stars will be adopted as members, but a few of them have motions that deviate enough from those of the Taurus groups that they could be unrelated young stars from Cas-Tau.

Each of the candidates from the preceding analysis was selected to reside within one of the nine Taurus fields and to have a similar parallax and proper motion as one of the populations of known members within its field. To search for candidates at larger distances from those populations, I have identified stars at any location within Figure 1 that satisfy the previously applied thresholds of parallax and proper motion for any of the populations of members. These relaxed criteria produce an additional 51 candidates that appear within the sequence of known members in color-magnitude diagrams. Most of these candidates are far from the populations to which they were matched ($> 5^\circ$) and are near the thresholds for parallax and proper motion, and thus are unlikely to be members. The remaining (eight) candidates agree more closely with the astrometry for the known populations and are within a few degrees of the boundaries of their fields. The latter candidates have been included in Table 6.

Four of the candidates comprise two $2''$ pairs, which correspond to 2MASS J04572852+3029107 and 2MASS J04355568+1707395. In addition, 2MASS J04161407+2758275, 2MASS J04291717+1826375, and 2MASS J05010116+2501413 are $0''.9$, $1''.4$, and $1''.8$ pairs, respectively, in which one component was selected as a candidate and the other one was rejected by the criteria for parallax or proper motion. The rejected component in the first pair has a poor astrometric fit, perhaps due to the binarity, and the rejected stars in the other two pairs are only slightly beyond the thresholds for selection in proper motion. 2MASS J04411296+1813194 is a $2''.3$ pair in which one component is a candidate and the other

one lacks parallax and proper motion measurements from *Gaia*. Only the components of these various pairs that were identified as candidates are listed in Table 6.

5. PROPERTIES OF THE STELLAR POPULATION

Gaia DR2 has made it possible to produce a highly refined census of known members of Taurus and to perform a thorough search for undiscovered members, which in turn should enable the best constraints to date on the distributions of masses and ages in the region.

5.1. Distribution of Ages

Because low-mass stars ($\lesssim 1 M_{\odot}$) are predicted to evolve primarily in a vertical direction in the Hertzsprung-Russell diagram for at least 10 Myr following their birth, the distribution of ages in a star-forming region should be directly reflected in a spread in luminosities at a given effective temperature. However, additional factors can contribute to the observed spread in luminosity estimates (Hartmann 2001), including unresolved binaries, uncorrected emission from circumstellar material, variations in distances to the stars (if a single distance is adopted for a population), uncertainties in photometry, extinctions, and bolometric corrections, and differences in accretion histories (Baraffe et al. 2009; Littlefair et al. 2011). Nevertheless, the luminosity spread in a star-forming region can provide useful constraints on the distribution of ages (Ballesteros-Paredes et al. 1999).

For a given star, I use the offset in its extinction-corrected M_J relative to the median sequence for Taurus, $\Delta M_J = M_J - M_J(\text{median})$, as a proxy for its relative age. The J band is selected for measuring the photospheric flux as a compromise between shorter wavelengths where disk emission is lower and longer wavelengths where extinction is lower. I have computed ΔM_J for known members of Taurus (Section 2.3) that have spectral types between K0–M7, estimates of extinction (Esplin & Luhman 2017; Luhman et al. 2017), and parallax measurements from *Gaia* DR2 that have errors of $\leq 10\%$ and that are not discrepant (Section 2.2). Stars with known edge-on disks, most protostars, and some close companions lack extinction estimates or spectral classifications, and hence are excluded. In addition, I have estimated ΔM_J for the candidate members identified in the previous section (Table 6). Each candidate was dereddened to the Pleiades locus in $J - H$ versus $G_{\text{RP}} - K_s$ to derive its extinction. The dereddened value of $G_{\text{RP}} - K_s$ was used to estimate the spectral type via comparison to the relation between $G_{\text{RP}} - K_s$ and spectral type for members of Upper Sco (Luhman et al. 2018). Since knowledge of the multiplicity of the members and candidates is incomplete, M_J was calculated for all stars in a uniform manner by using seeing-limited photometry from 2MASS and UKIDSS.

The distributions of ΔM_J for known members and candidates are shown in Figure 19. Separate distributions are included for diskless and disk-bearing members (Esplin et al. 2014; Esplin & Luhman 2017). One might expect that members with disks would be brighter on average if they are younger or if disk emission contributes to the observed fluxes, but the two populations exhibit similar distributions of ΔM_J . Because of the requirement of a parallax measurement from *Gaia*, which oper-

ates at optical wavelengths, the most heavily reddened members are absent from Figure 19, which tend to be the youngest and least evolved stars. For instance, most of the ~ 40 protostars in Taurus lack parallax measurements. Many of them also lack spectral classifications or reliable estimates of their extinction-corrected photospheric fluxes.

The M_J offset of the median sequence of Upper Sco (11 Myr, Pecaut et al. 2012) relative to Taurus is marked in Figure 19. The value of that offset is ~ 1.2 mag, which implies that Taurus is younger by a factor of ~ 5 according to evolutionary models of low-mass stars (Siess et al. 2000; Baraffe et al. 1998, 2015). Very few members of Taurus are fainter than the median of Upper Sco, which suggests that the number of members with ages of $\gtrsim 10$ Myr is quite small. The true number in that age range may be even smaller than implied by Figure 19 given that some of the faint disk-bearing stars could have erroneous estimates of their intrinsic fluxes because of scattered light while a few of the faint diskless stars could be members of Cas-Tau that happen to overlap with Taurus in parallax and proper motion (see Fig. 14). Measurements of radial velocities for the faintest stars in Figure 19 would be useful to further constrain their membership. Meanwhile, the distribution of ΔM_J for the 54 candidates from the previous section is somewhat fainter on average than the known members, indicating older ages. This difference is a reflection of the fact that a majority of the candidates are associated with the blue and cyan populations in L1551 and L1517, whose known members have older median ages than the median of Taurus as a whole (Figs. 8 and 9).

The paucity of stars at ages of $\gtrsim 10$ Myr in Figure 19 is consistent with previous studies of the distribution of ages in Taurus (Ballesteros-Paredes et al. 1999; Hartmann 2001). The analysis in this work benefits from a larger and more refined sample of members and better determined completeness at older ages. Since the stellar populations within Taurus and other molecular clouds appeared to contain few stars at $\gtrsim 10$ Myr and most clouds show evidence of star formation, Ballesteros-Paredes et al. (1999) and Hartmann et al. (2001) concluded that the formation of molecular clouds, the birth of stars within them, and the dispersal of the clouds all occur rapidly on a timescale of a few Myr. They found that the small age spread in Taurus was particularly enlightening since it is much smaller than the crossing time of the region (few Myr vs. 10–20 Myr), further indicating that molecular clouds form rapidly, probably through converging flows of atomic gas. The presence of a small number of older stars is consistent with that scenario (Hartmann et al. 2012).

5.2. Initial Mass Function

Previous estimates of the IMF in Taurus have been restricted to specific areas for which the completeness of the stellar census appeared to be well-defined (Briceno et al. 2002; Luhman et al. 2003a; Luhman 2004; Luhman et al. 2009). For my analysis, I have considered the fields in Figures 2–11, which were searched for new members in Section 4. Those fields are large enough to encompass all of the Taurus clouds and nearly all of the known members.

A reliable estimate of the IMF in a stellar population

requires a sample of members that is likely to be unbiased in mass. To identify the selection criteria for such a sample in Taurus, I examine the completeness of my *Gaia* survey for new members. In *Gaia* DR2, most stars have parallax measurements down to $G \sim 19$, and the fraction with parallaxes quickly decreases at fainter magnitudes (Gaia Collaboration et al. 2018b). For instance, the percentage of stars in the Taurus fields with parallax errors of ≤ 0.7 mas ($\lesssim 10\%$ error at the distance of Taurus) is $\sim 80\%$ and $\sim 20\%$ near $G = 19$ and 20, respectively. The mass (or spectral type) that corresponds to a given limit in G is a function of extinction, which varies significantly among members of Taurus. The range of spectral types and extinctions in which Taurus members have *Gaia* parallaxes is illustrated in Figure 20, which shows extinction versus spectral type for members at K0–L0. Different symbols are used for stars with parallaxes that have errors of $\leq 10\%$ and that are not discrepant (Section 2.2) and the remaining members above and below the magnitude of $G \sim 19$ beyond which precise parallaxes become unavailable. Those three samples contain 289, 44, and 44 stars, respectively. Some members cannot be included in Figure 20 because they lack spectral types or extinction estimates, which consist of stars with edge-on disks, most protostars, and some companions. Six of the known members are bright enough at optical wavelengths that they should be easily detected by *Gaia* but do not appear in DR2, consisting of HL Tau, XEST 17-059, J2-2041, V927 Tau, IRAS 04248+2612, and IRAS 04264+2433. Most of these stars have companions or extended emission that can account for their absences from DR2. They are excluded from Figure 20. Similarly, the 44 members in DR2 that have $G \leq 19$ but lack parallax measurements have poor astrometric fits, likely due to companions or extended emission.

In Figure 20, the interface between stars with precise parallaxes and stars at $G > 19$ that lack parallaxes (filled circles and open triangles) roughly approximates the magnitude of $G \sim 19$ below which precise parallaxes become unavailable due to insufficient flux. That interface extends from $\sim M9$ at $A_J = 0$ to mid-M types at $A_J = 3$. I would like to define the IMF sample with an extinction limit that is high enough to encompass a large number of members but low enough that the sample has a high level of completeness for *Gaia* parallaxes down to a relatively late spectral type. Given these considerations, I have selected members with $A_J < 1$ for the IMF sample. As shown in Figure 20, that extinction limit intersects the $G \sim 19$ interface at $\sim M6$ – $M7$, so the *Gaia* parallaxes (and hence the survey for new members) should be mostly complete for members within those extinction and spectral type limits. The completeness limit in spectral type at $A_J = 1$ is somewhat uncertain given the sparse distribution of known late-type members near that extinction. The more conservative limit of M6 is shown in Figure 21. If the extinctions of members are independent of mass and spectral type, then this extinction-limited sample should be unbiased in mass and representative of the Taurus population. As mentioned above, some known members at $G \leq 19$ lack *Gaia* parallaxes, so the same could be true for undiscovered members. However, the presence of extended emission is one of the reasons that known members lack parallaxes, but that is unlikely to be the case for undiscovered members given

that the census of disk-bearing members should be nearly complete (Esplin et al. 2014). In addition, most of the known members that have erroneous astrometry due to binarity have spectral types of late-K or early M, whereas most undiscovered members probably have later spectral types, which are less prone to binarity-induced astrometric errors due to their lower binary fractions and smaller separations (Duchêne & Kraus 2013).

For the IMF sample in Taurus, I have selected all known members that have extinction estimates of $A_J \leq 1$ and spectral classifications, which corresponds to 295 objects. To avoid some of the sources of uncertainty in estimating masses of young stars, I use the distribution of spectral types in the sample as a proxy for the IMF. In the top panel of Figure 21, I show the distribution reported by Luhman et al. (2009) for 26 fields observed by the *XMM-Newton* Extended Survey of the Taurus Molecular Cloud (XEST, Güdel et al. 2007), which have diameters of $\sim 0.5^\circ$ and are centered on the stellar aggregates. The second panel presents the distribution for my extinction-limited sample of 295 members across all of Taurus. That panel also includes the distribution produced after adding the candidate members with $A_J \leq 1$ from Section 4 (Table 6) using the spectral types and extinctions estimated in Section 5.1. For comparison to Taurus, I show distributions for an extinction-limited sample in IC 348 (Luhman et al. 2016) and a sample of stars in the ONC in the bottom two panels in Figure 21. The ONC sample consists of stars from the spectroscopic census from Hillenbrand et al. (2013) that are within the $33' \times 33'$ field considered by Da Rio et al. (2012) and additional stars in that field for which photometric spectral types were estimated by Da Rio et al. (2012). Those photometric types should have a high level of completeness down to $\sim M5$ according to the analysis in Da Rio et al. (2012). The field from that study was selected for comparison to Taurus because it should be large enough to contain a representative sample of members that is not affected by mass segregation.

As mentioned in Section 1 and illustrated in Figure 21, previous samples of Taurus members in small fields like those in the XEST survey have exhibited a surplus of K7–M0 stars (0.7 – $0.8 M_\odot$) relative to denser clusters like IC 348 and the ONC. However, the spectral type distribution for the entirety of Taurus does not contain a surplus of that kind, and instead resembles the distributions in IC 348 and the ONC, particularly when the candidates from Section 4 are included. Many of the stars with types of K7–M0 in older studies have new classifications that are later by 1–3 subclasses (Herczeg & Hillenbrand 2014; Luhman et al. 2017, references therein), which is partially responsible for the disappearance of the K7–M0 surplus. Mass segregation also appears to be present in which K7–M0 stars are more likely to be located in smaller areas surrounding the aggregates than the less massive stars. Thus, the stellar IMF exhibits little variation between Taurus, IC 348, and the ONC, which span 3–4 orders of magnitude in stellar density.

6. CONCLUSIONS

The high-precision astrometry from DR2 of the *Gaia* mission has been used to improve the census of members of the Taurus star-forming region. The results are summarized as follows.

1. Parallaxes and proper motions are available from *Gaia* DR2 for 76% of the stars adopted as Taurus members by Esplin & Luhman (2017). I have used those data to characterize the kinematics and distances of the groups associated with the Taurus clouds and to check for nonmembers within that sample. After including additional stars that show evidence of membership from *Gaia* and previous spectral classifications, the revised catalog of members contains 438 objects.
2. The young stars KPNO 15 and 2MASS J04355209+2255039 have discrepant proper motions relative to the group in L1536 that they are projected against. According to their *Gaia* proper motions, they were near the same location within the cloud ~ 7200 years ago, indicating that they may have been participants in a dynamical interaction that resulted in their ejection.
3. Kraus et al. (2017) and Zhang et al. (2018) presented samples of stars that appear to be older than the known members of Taurus ($\gtrsim 10$ Myr) and that they classified as members of the region. Among those older stars that have *Gaia* parallaxes and proper motions, none have kinematics and distances that are consistent with a physical relationship with the Taurus groups.
4. A subset of the older stars from Kraus et al. (2017) form a cluster in parallax and proper motion that coincides with a possible new moving group of nine stars found with *Gaia* DR1 by Oh et al. (2017). I have identified 91 candidate members of this group using DR2. They have distances of 116–127 pc and an age of ~ 40 Myr based on a comparison to Tuc-Hor (45 Myr, Bell et al. 2015).
5. I have performed a search for new members of Taurus by selecting stars from *Gaia* DR2 that have proper motions and distances that are similar to those of any of the groups of known members. The resulting candidates exhibit two distinct populations, one that is within the range of ages of the known members ($\lesssim 10$ Myr) and another that is much older ($\gtrsim 40$ Myr). The latter population is consistent with field stars that are unrelated to the Taurus clouds.
6. Relative ages of the known members and candidate members have been characterized using their offsets in M_J from the median sequence for Taurus. Very few members or candidates are fainter (older) than the median sequence of Upper Sco (11 Myr), which contradicts previous reports of a significant population of older stars ($\gtrsim 10$ Myr) associated with the Taurus groups. The absence of an older population reinforces the previous evidence that molecular clouds form rapidly on a timescale of a few Myr (Ballesteros-Paredes et al. 1999; Hartmann et al. 2001, 2012).
7. Previous estimates of the IMF within small fields surrounding the Taurus aggregates have exhibited a surplus of K7–M0 stars ($0.7\text{--}0.8 M_\odot$) relative

to star-forming clusters like IC 348 and the ONC (Briceño et al. 2002; Luhman et al. 2003a; Luhman 2004; Luhman et al. 2009). However, that surplus is absent from the new census for the entire region. Thus, the stellar IMF exhibits little variation among nearby star-forming regions spanning 3–4 orders of magnitude in stellar density.

I thank Eric Mamajek for comments on the manuscript. This work has made use of data from the European Space Agency (ESA) mission *Gaia* (<https://www.cosmos.esa.int/gaia>), processed by the *Gaia* Data Processing and Analysis Consortium (DPAC, <https://www.cosmos.esa.int/web/gaia/dpac/consortium>). Funding for the DPAC has been provided by national institutions, in particular the institutions participating in the *Gaia* Multilateral Agreement. 2MASS is a joint project of the University of Massachusetts and IPAC at Caltech, funded by NASA and the NSF. The Center for Exoplanets and Habitable Worlds is supported by the Pennsylvania State University, the Eberly College of Science, and the Pennsylvania Space Grant Consortium.

REFERENCES

- Abt, H. A. 2004, *ApJS*, 155, 175
- Ballesteros-Paredes, J., Hartmann, L., & Vázquez-Semadeni, E. 1999, *ApJ*, 527, 285
- Baraffe, I., Chabrier, G., Allard, F., & Hauschildt, P. H. 1998, *A&A*, 337, 403
- Baraffe, I., Chabrier, G., & Gallardo, J. 2009, *ApJ*, 702, L27
- Baraffe, I., Horneier, D., Allard, F., & Chabrier, G. 2015, *A&A*, 577, 42
- Barnard, E. E., Frost, E. B., & Calvert, M. R. 1927, *A Photographic Atlas of Selected Regions of the Milky Way* (Washington, DC: Carnegie Inst.)
- Beichman, C. A., Myers, P. C., Emerson, J. P., et al. 1986, *ApJ*, 307, 337
- Bell, C. P. M., Mamajek, E. E., & Naylor, T. 2015, *MNRAS*, 454, 593
- Bertout, C., & Genova, F. 2006, *A&A*, 460, 499
- Blaauw, A. 1956, *ApJ*, 132, 408
- Bonavita, M., Daemgen, S., Desidera, S., et al. 2014, *ApJ*, 791, L40
- Bonnell, I. A., Smith, R. J., Clark, P. C., & Bate, M. R. 2011, *MNRAS*, 410, 2339
- Briceño, C., Calvet, N., Kenyon, S., & Hartmann, L. 1999, *AJ*, 118, 1354
- Briceño, C., Hartmann, L., Stauffer, J., & Martín, E. L., 1998, *AJ*, 115, 2074
- Briceño, C., Hartmann, L., Stauffer, J., et al. 1997, *AJ*, 113, 740
- Briceño, C., Luhman, K. L., Hartmann, L., Stauffer, J. R., & Kirkpatrick, J. D. 2002, *ApJ*, 580, 317
- Cui, X. Q., Zhao, Y. H., Chu, Y. Q., et al. 2012, *RA&A*, 12, 1197
- Daemgen, S., Bonavita, M., Jayawardhana, R., Lafrenière, D., & Janson, M. 2015, *ApJ*, 799, 155
- Dahm, S. E. 2015, *ApJ*, 813, 108
- Danielski, C., Babusiaux, C., Ruiz-Dern, L., Sartoretti, P., & Arenou, F. 2018, *A&A*, 614, A19
- Da Rio, N., Robberto, M., Hillenbrand, L. A., Henning, T., & Stassun, K. G. 2012, *ApJ*, 748, 14
- David, T. J., Mamajek, E. E., Vanderburg, A., et al. 2018, *ApJ*, submitted
- de Bruijne, J. H. J. 2012, *Ap&SS*, 341, 31
- de Bruijne, J. H. J., & Eilers, A.-C. 2012, *A&A*, 546, A61
- de Zeeuw, P. T., Hoogerwerf, R., de Bruijne, J. H. J., Brown, A. G. A., & Blaauw, A. 1999, *AJ*, 117, 354
- Dobashi, K., Uehara, H., Kandori, R., et al. 2005, *PASJ*, 57, 1
- Duchêne, G., & Kraus, A. 2013, *ARA&A*, 51, 269
- Esplin, T. L., & Luhman, K. L. 2017, *AJ*, 154, 134
- Esplin, T. L., & Luhman, K. L. in preparation
- Esplin, T. L., Luhman, K. L., & Mamajek, E. E. 2014, *ApJ*, 784, 126
- Feiden, G. A. 2016, *A&A*, 593, A99
- Frink, S., Röser, S., Neuhäuser, R., & Sterzik, M. F. 1997, *A&A*, 325, 613
- Gagné, J., Mamajek, E. E., Malo, L., et al. 2018, *ApJ*, 856, 23
- Gaia Collaboration, Babusiaux, C., van Leeuwen, F., Barstow, M. A., et al. 2018a, *A&A*, 616, A10
- Gaia Collaboration, Brown, A. G. A., Vallenari, A., Prusti, T., et al. 2018b, *A&A*, 616, A1
- Galli, P. A. B., Loinard, L., Ortiz-Léon, G. N., et al. 2018, *ApJ*, 859, 33
- Gomez, M., Jones, B. F., Hartmann, L., et al. 1992, *AJ*, 104, 762
- Gontcharov, G. A. 2006, *AstL*, 32, 759
- Güdel, M., Briggs, K. R., Arzner, K., et al. 2007, *A&A*, 468, 353
- Guieu, S., Dougados, C., Monin, J.-L., Magnier, E. & Martín, E. L. 2006, *A&A*, 446, 485
- Hartigan, P., & Kenyon, S. J. 2003, *ApJ*, 583, 334
- Hartmann, L. 2001, *AJ*, 121, 1030
- Hartmann, L. 2003, *ApJ*, 585, 398
- Hartmann, L., Ballesteros-Paredes, J., & Bergin, E. A. 2001, *ApJ*, 562, 852
- Hartmann, L., Ballesteros-Paredes, J., & Heitsch, F. 2012, *MNRAS*, 420, 1457
- Hartmann, L., Calvet, N., Watson, D. M., et al. 2005, *ApJ*, 628, L147
- Hartmann, L., Hewett, R., Stahler, S., & Mathieu, R. D. 1986, *ApJ*, 309, 275
- Hartmann, L., Jones, B. F., Stauffer, J. R., & Kenyon, S. J. 1991, *AJ*, 101, 1050
- Henry, T. J., Kirkpatrick, J. D., & Simons, D. A. 1994, *AJ*, 108, 1437
- Herczeg, G. J., & Hillenbrand, L. A. 2014, *ApJ*, 786, 97
- Hillenbrand, L. A. 1997, *AJ*, 113, 1733
- Hillenbrand, L. A., & Carpenter, J. M. 2000, *ApJ*, 540, 236
- Hillenbrand, L. A., Hoffer, A. S., & Herczeg, G. J. 2013, *AJ*, 146, 85
- Ireland, M. J., & Kraus, A. L. 2008, *ApJ*, 678, L59
- Johnson D. R. H., & Soderblom D. R., 1987, *AJ*, 93, 864
- Kaiser, N., Aussel, H., Burke, B. E., et al. 2002, *Proc. SPIE*, 4836, 154
- Kaiser, N., Burgett, W., Chambers, K., et al. 2010, *Proc. SPIE*, 7733, 12
- Kenyon, S. J., Gómez, M., & Whitney, B. A. 2008, *Handbook of Star Forming Regions, Volume 1, ASP Monograph Series*, 405
- Kenyon, S. J., Hartmann, L. W., Strom, K. M., & Strom, S. E. 1990, *AJ*, 99, 869
- Kirkpatrick, J. D., Henry, T. J., & Irwin, M. J. 1997, *AJ*, 113, 1421
- Kirkpatrick, J. D., Henry, T. J., & McCarthy, D. W. 1991, *ApJS*, 77, 417
- Kounkel, M., Covey, K., Suárez, G., et al. 2018, *AJ*, 156, 84
- Kraus, A. L., Herczeg, G. J., Rizzuto, A. C., et al. 2017, *ApJ*, 838, 150
- Kraus, A. L., Ireland, M. J., Martinache, F., & Hillenbrand, L. A. 2011, *ApJ*, 731, 8
- Lawrence, A., Warren, S. J., Almaini, O., et al. 2007, *MNRAS*, 379, 1599
- Leinert, C., Zinnecker, H., Weitzel, N., et al. 1993, *A&A*, 278, 129
- Littlefair, S. P., Naylor, T., Mayne, N. J., Saunders, E., Jeffries, R. D. 2011, *MNRAS*, 413, L56
- Loinard, L., Mioduszewski, A. J., Rodríguez, L. F., et al. 2005, *ApJ*, 619, L179
- Loinard, L., Torres, R. M., Mioduszewski, A. J., et al. 2007, *ApJ*, 671, 546 619, L179
- Luhman, K. L. 1999, *ApJ*, 525, 466
- Luhman, K. L. 2004, *ApJ*, 617, 1216
- Luhman, K. L. 2006, *ApJ*, 645, 676
- Luhman, K. L. 2012, *ARA&A*, 50, 65
- Luhman, K. L., Allen, P. R., Espaillat, C., Hartmann, L., & Calvet, N. 2010, *ApJS*, 186, 111
- Luhman, K. L., Briceño, C., Rieke, G. H., Hartmann, L. 1998a, *ApJ*, 493, 909
- Luhman, K. L., Briceño, C., Stauffer, J. R., et al. 2003a, *ApJ*, 590, 348
- Luhman, K. L., Esplin, T. L., & Loutrel, N. P. 2016, *ApJ*, 827, 52
- Luhman, K. L., Herrmann, K. A., Mamajek, E. E., Esplin, T. L., & Pecaut, M. J. 2018, *AJ*, 156, 76
- Luhman, K. L., Liebert, J., & Rieke, G. H. 1997, *ApJ*, 489, L165
- Luhman, K. L., Mamajek, E. E., Allen, P. R., & Cruz, K. L. 2009, *ApJ*, 703, 399
- Luhman, K. L., Mamajek, E. E., Shukla, S. J., & Loutrel, N. P. 2017, *AJ*, 153, 46
- Luhman, K. L., Rieke, G. H., Lada, C. J., & Lada, E. A. 1998b, *ApJ*, 508, 347
- Luhman, K. L., Stauffer, J. R., Muench, A. A., et al. 2003b, *ApJ*, 593, 1093
- Luhman, K. L., Whitney, B. A., Meade, M. R., et al. 2006, *ApJ*, 647, 1180
- Lynds, B. T. 1962, *ApJS*, 7, 1
- Martín, E. L., & Magazzù, A. 1999, *A&A*, 342, 173
- Mathieu, R. D., Stassun, K., Basri, G., et al. 1997, *AJ*, 113, 1841
- Muench, A. A., Lada, E. A., Lada, C. J., & Alves, J. 2002, *ApJ*, 573, 366
- Muench, A. A., Lada, E. A., Lada, C. J., et al. 2003, *AJ*, 125, 2029
- Muzerolle, J., Hillenbrand, L., Calvet, N., Briceño, C., & Hartmann, L. 2003, *ApJ*, 592, 266
- Neuhäuser, R., Sterzik, M. F., Schmitt, J. H. M. M., Wichmann, R., & Krautter, J. 1995, *A&A*, 295, L5
- Nguyen, D. C., Brandeker, A., Van Kerkwijk, M. H., & Jayawardhana, R. 2012, *ApJ*, 745, 119

- Oh, S., Price-Whelan, A. M., Hogg, D. W., Morton, T. D., & Spergel, D. N. 2017, *AJ*, 153, 257
- Onishi, T., Mizuno, A., Kawamura, A., Tachihara, K., & Fukui, Y. 2002, *ApJ*, 575, 950
- Pecaut M. J., Mamajek E. E., & Bubar E. J. 2012, *ApJ*, 746, 154
- Perryman, M. A. C., de Boer, K. S., Gilmore, G., et al. 2001, *A&A*, 369, 339
- Poveda, A., Ruiz, J., & Allen, C. 1967, *Bol. Obs. Tonantzintla Tacubaya*, 4, 86
- Racine, R. 1968, *AJ*, 73, 233
- Rebull, L. M., Padgett, D. L., McCabe, C. E., et al. 2010, *ApJS*, 186, 259
- Reipurth, B., Lindgren, H., Nordstrom, B., & Mayor, M. 1990, *A&A*, 235, 197
- Rice, E. L., Barman, T., McLean, I. S., Prato, L., & Kirkpatrick, J. D. 2010, *ApJS*, 186, 63
- Scelsi, L., Sacco, G., Affer, L., et al. 2008, *A&A*, 490, 601
- Sestito, P., Palla, F., & Randich, S. 2008, *A&A*, 487, 965
- Siess, L., Dufour, E., & Forestini, M. 2000, *A&A*, 358, 593
- Skrutskie, M., Cutri, R. M., Stiening, R., et al. 2006, *AJ*, 131, 1163
- Slesnick, C. L., Carpenter, J. M., Hillenbrand, L. A., & Mamajek, E. E. 2006, *AJ*, 132, 2665
- Stassun, K. G., & Torres, G. 2018, *ApJ*, 862, 61
- Stauffer, J. R., Hartmann, L. W., Fazio, G. G., et al. 2007, *ApJS*, 172, 663
- Torres, G., Ruíz-Rodríguez, D., & Badenas, M. et al. 2013, *ApJ*, 773, 40
- Torres, R. M., Loinard, L., Mioduszewski, A. J., et al. 2007, *ApJ*, 671, 1813
- Torres, R. M., Loinard, L., Mioduszewski, A. J., et al. 2009, *ApJ*, 698, 242
- Torres, R. M., Loinard, L., Mioduszewski, A. J., et al. 2012, *ApJ*, 747, 18
- Walter, F. M., Brown, A., Mathieu, R. D., Myers, P. C., & Vrba, F. J. 1988, *AJ*, 96, 297
- Werner, M. W., Roellig, T. L., Low, F. J., et al. 2004, *ApJS*, 154, 1
- White, R. J., & Basri, G. 2003, *ApJ*, 582, 1109
- White, R. J., & Ghez, A. M. 2001, *ApJ*, 556, 265
- White, R. J., & Hillenbrand, L. A. 2005, *ApJ*, 621, L65
- Wichmann, R., Krautter, J., Schmitt, J. H. M. M., et al. 1996, *A&A*, 312, 439
- Wichmann, R., Torres, G., Melo, C. H. F., et al. 2000, *A&A*, 359, 181
- Wright, E. L., Eisenhardt, P. R. M., Mainzer, A. K., et al. 2010, *AJ*, 140, 1868
- Yu, L., Donati, J.-F., Hebrard, E. M., et al. 2017, *MNRAS*, 467, 1342
- Zhang, Z., Liu, M. C., Best, W. M. J., et al. 2018, *ApJ*, 858, 41
- Zhao, G., Zhao Y. H., Chu Y. Q., Jing Y. P., Deng L. C., 2012, *RA&A*, 12, 723

TABLE 1
MEMBERS OF TAURUS

Column Label	Description
2MASS	2MASS Point Source Catalog source name
UGCS	UKIDSS Galactic Clusters Survey source name ^a
Names	Other source names
RAdeg	Right ascension (J2000)
DEdeg	Declination (J2000)
Ref-Pos	Reference for right ascension and declination ^b
SpType	Adopted spectral type ^c
pmRA	Proper motion in right ascension from <i>Gaia</i> DR2
e_pmRA	Error in pmRA
pmDec	Proper motion in declination from <i>Gaia</i> DR2
e_pmDec	Error in pmDec
plx	Parallax from <i>Gaia</i> DR2
e_plx	Error in plx
RVel	Radial velocity
e_RVel	Error in RVel
r_RVel	Radial velocity reference ^d
U	<i>U</i> component of space velocity
e_U	Error in U
V	<i>V</i> component of space velocity
e_V	Error in V
W	<i>W</i> component of space velocity
e_W	Error in W
Gmag	<i>G</i> magnitude from <i>Gaia</i> DR2
e_Gmag	Error in Gmag
GBPmag	<i>G</i> _{BP} magnitude from <i>Gaia</i> DR2
e_GBPmag	Error in GBPmag
GRPmag	<i>G</i> _{RP} magnitude from <i>Gaia</i> DR2
e_GRPmag	Error in GRPmag
Pop	Population ^e

NOTE. — The table is available in a machine-readable form.

^a Based on coordinates from Data Release 10 of the UKIDSS Galactic Clusters Survey for stars with $K_s > 10$ from the Two Micron All Sky Survey (2MASS, Skrutskie et al. 2006).

^b Sources of the right ascension and declination are *Gaia* DR2, the 2MASS Point Source Catalog, UKIDSS Data Release 10, and images from the *Spitzer Space Telescope* (Luhman et al. 2010).

^c Spectral types adopted by Luhman et al. (2017) and Esplin & Luhman (2017) with the exception of HD 283641, RX J0422.1+1934, L1551-55, RX J0507.2+2437, HD 28354, HD 283782, HD 30378, PSO J065.8871+19.8386/PSO J071.6033+17.0281/PSO J074.1999+29.2197, and PSO J071.3189+31.6888/PSO J076.2495+31.7503, whose types are from Wichmann et al. (2000), Martín & Magazzù (1999), Herczeg & Hillenbrand (2014), Briceño et al. (1999), Abt (2004), Wichmann et al. (1996), Racine (1968), Esplin & Luhman (2018), and this work, respectively.

^d (1) Nguyen et al. (2012); (2) Gontcharov (2006); (3) Muzerolle et al. (2003); (4) White & Basri (2003); (5) Torres et al. (2013); (6) Hartmann et al. (1986); (7) Wichmann et al. (2000); (8) Kraus et al. (2017); (9) Reipurth et al. (1990); (10) Rice et al. (2010); (11) Scelsi et al. (2008); (12) Mathieu et al. (1997); (13) *Gaia* DR2.

^e Populations in Figures 2–11.

TABLE 2
 MEDIAN PARALLAXES AND PROPER MOTIONS FOR POPULATIONS IN FIGURES 2–10

Figure	Pop	Clouds in Figure	π^a (mas)	μ_α^a (mas yr ⁻¹)	μ_δ^a (mas yr ⁻¹)	$\Delta\mu_\alpha^b$ (mas yr ⁻¹)	$\Delta\mu_\delta^b$ (mas yr ⁻¹)	$\sigma(\mu_\alpha)^c$ (mas yr ⁻¹ /km s ⁻¹)	$\sigma(\mu_\delta)^c$ (mas yr ⁻¹ /km s ⁻¹)	N*
2	red	B209	7.6	8.5	-24.4	-2.4	-1.0	1.0/0.6	1.5/0.9	22
2	blue	B209	6.3	12.1	-17.9	3.0	2.1	0.7/0.5	1.2/0.9	4
3	red	L1495	7.8	8.7	-25.5	-1.8	-0.9	1.5/0.9	1.1/0.7	31
4	red	L1521/B213/B215	7.6	8.0	-23.2	-1.5	-0.1	2.0/1.2	2.8/1.7	36
4	blue	L1521/B213/B215	6.2	11.0	-17.7	3.1	1.5	4.2/3.2	1.7/1.3	24
5	red	L1527	7.1	5.9	-20.6	-0.9	0.3	1.8/1.2	2.7/1.8	24
6	red	L1524/L1529/L1536	7.8	7.2	-21.4	-1.0	1.5	1.8/1.1	1.2/0.7	34
6	blue	L1524/L1529/L1536	6.2	10.1	-16.8	3.6	0.8	1.5/1.1	3.1/2.4	33
7	blue	L1489/L1498	6.7	14.1	-18.8	3.3	0.9	0.9/0.6	0.5/0.4	4
8	red	L1551/L1558	6.9	6.8	-12.4	-2.2	5.8	2.3/1.6	1.5/1.0	5
8	blue	L1551/L1558	6.9	12.0	-18.6	4.6	-1.6	1.3/0.9	1.3/0.9	40
8	green	L1551/L1558	5.1	4.8	-13.9	0.6	-1.3	0.6/0.6	0.3/0.3	5
9	cyan	L1517	6.3	4.7	-24.5	0.7	-3.7	0.8/0.6	1.7/1.3	32
10	cyan	L1544	5.8	2.7	-17.6	0.0	-0.4	1.6/1.3	2.7/2.2	11

^a Based on data from *Gaia* DR2.

^b For a given star, $\Delta\mu$ is defined as the difference between the *Gaia* DR2 proper motion and the proper motion expected for the position and parallax of the star assuming the median space velocity of Taurus members from Section 2.3 ($\mu - \text{expected } \mu$ in Figures 2–10).

^c Standard deviation of the proper motions and the corresponding velocity at the median distance of the population.

TABLE 3
 MEDIAN ASTROMETRIC AND KINEMATIC PARAMETERS FOR TAURUS AGGREGATES

Population/Cloud	α (J2000) (deg)	δ (J2000) (deg)	π^a (mas)	μ_α^a (mas yr ⁻¹)	μ_δ^a (mas yr ⁻¹)	U^b	V^b	W^b	σ_U	σ_V	σ_W	N*
						(km s ⁻¹)			(km s ⁻¹)			
red/B209	63.57	28.19	7.7	8.4	-24.3	-15.5	-11.8	-10.6	2.4	0.7	1.3	6
red/L1495	64.73	28.40	7.8	8.7	-25.5	-15.8	-12.0	-10.7	1.9	1.2	0.9	14
red/L1521	67.45	26.06	7.6	6.2	-26.0	-15.1	-10.5	-9.6	1.8	1.2	1.3	8
red/L1527	69.60	25.94	7.2	5.1	-26.8	-15.9	-12.0	-10.5	2.5	1.5	0.6	4
red/L1524/L1529	68.56	24.30	7.8	7.2	-21.2	-15.8	-11.1	-9.3	1.1	0.7	1.0	16
blue/L1536	68.96	22.84	6.2	8.4	-21.1	-16.8	-13.5	-6.8	1.1	1.3	2.0	10
blue/L1551	68.06	18.22	6.9	12.0	-18.5	-15.9	-14.7	-7.6	1.6	1.0	0.9	18
green/L1558	71.75	17.00	5.1	4.8	-20.1	-18.9	-13.9	-10.6	0.6	0.3	0.3	3
cyan/L1517	73.94	30.37	6.3	4.3	-24.1	-15.0	-14.7	-10.4	3.3	1.2	0.9	5

^a Based on data from *Gaia* DR2.

^b Based on *UVW* from Table 1. The 100 members with estimates of *UVW* have a median value of $-15.9, -12.4, -9.4$ km s⁻¹.

TABLE 4
 SINGLE-STAR SEQUENCES FOR THE β PIC
 MOVING GROUP, THE TUC-HOR
 ASSOCIATION, AND THE PLEIADES CLUSTER

$G_{\text{BP}} - G_{\text{RP}}$	$M_{G_{\text{BP}}}$		
	β Pic	Tuc-Hor	Pleiades
0.0	1.40	1.40	1.40
0.1	1.75	1.75	1.75
0.2	2.05	2.05	2.05
0.3	2.25	2.25	2.25
0.4	2.45	2.45	2.45
0.5	2.80	2.80	2.80
0.6	3.15	3.15	3.15
0.7	3.47	3.75	3.75
0.8	3.80	4.20	4.20
0.9	4.05	4.60	4.60
1.0	4.30	5.00	5.00
1.1	4.60	5.20	5.35
1.2	4.90	5.34	5.65
1.3	5.17	5.57	5.90
1.4	5.45	5.80	6.15
1.5	5.65	6.00	6.40
1.6	5.85	6.20	6.60
1.7	6.00	6.37	6.82
1.8	6.20	6.54	7.05
1.9	6.35	6.70	7.23
2.0	6.50	6.88	7.40
2.1	6.65	7.04	7.55
2.2	6.80	7.20	7.77
2.3	7.00	7.35	7.98
2.4	7.20	7.55	8.15
2.5	7.44	7.77	8.42
2.6	7.65	8.00	8.67
2.7	7.85	8.30	8.90
2.8	...	8.60	9.20
2.9	...	8.85	9.55
3.0	...	9.15	9.90
3.1	...	9.45	...
3.2	...	9.75	...
3.3	...	10.00	...
3.4	...	10.30	...

NOTE. — The fits are based on data from *Gaia* DR2 for members from Stauffer et al. (2007) and Bell et al. (2015, references therein). The data for the Pleiades were corrected for extinction assuming $A_V = 0.12$ (Stauffer et al. 2007) and the reddening relations from Danielski et al. (2018) and Gaia Collaboration et al. (2018a). The other two populations should have very little extinction ($A_V \sim 0.03$, Bell et al. 2015), so corrections were not applied to their data.

TABLE 5
CANDIDATE MEMBERS OF GROUP 29 FROM OH ET AL. (2017)

Column Label	Description
2MASS	2MASS Point Source Catalog source name
Name	Other source name
RAdeg	Right ascension from <i>Gaia</i> DR2 (J2000)
DEdeg	Declination from <i>Gaia</i> DR2 (J2000)
pmRA	Proper motion in right ascension from <i>Gaia</i> DR2
e_pmRA	Error in pmRA
pmDec	Proper motion in declination from <i>Gaia</i> DR2
e_pmDec	Error in pmDec
plx	Parallax from <i>Gaia</i> DR2
e_plx	Error in plx
Gmag	G magnitude from <i>Gaia</i> DR2
e_Gmag	Error in Gmag
GBPmag	G_{BP} magnitude from <i>Gaia</i> DR2
e_GBPmag	Error in GBPmag
GRPmag	G_{RP} magnitude from <i>Gaia</i> DR2
e_GRPmag	Error in GRPmag
Jmag	J magnitude from the 2MASS Point Source Catalog
e_Jmag	Error in Jmag
Hmag	H magnitude from the 2MASS Point Source Catalog
e_Hmag	Error in Hmag
Ksmag	K_s magnitude from the 2MASS Point Source Catalog
e_Ksmag	Error in Ksmag

NOTE. — The table is available in a machine-readable form.

TABLE 6
CANDIDATE MEMBERS OF TAURUS

Column Label	Description
2MASS	2MASS Point Source Catalog source name
RAdeg	Right ascension from <i>Gaia</i> DR2 (J2000)
DEdeg	Declination from <i>Gaia</i> DR2 (J2000)
pmRA	Proper motion in right ascension from <i>Gaia</i> DR2
e_pmRA	Error in pmRA
pmDec	Proper motion in declination from <i>Gaia</i> DR2
e_pmDec	Error in pmDec
plx	Parallax from <i>Gaia</i> DR2
e_plx	Error in plx
Gmag	G magnitude from <i>Gaia</i> DR2
e_Gmag	Error in Gmag
GBPmag	G_{BP} magnitude from <i>Gaia</i> DR2
e_GBPmag	Error in GBPmag
GRPmag	G_{RP} magnitude from <i>Gaia</i> DR2
e_GRPmag	Error in GRPmag
Jmag	J magnitude from the 2MASS Point Source Catalog
e_Jmag	Error in Jmag
Hmag	H magnitude from the 2MASS Point Source Catalog
e_Hmag	Error in Hmag
Ksmag	K_s magnitude from the 2MASS Point Source Catalog
e_Ksmag	Error in Ksmag

NOTE. — The table is available in a machine-readable form.

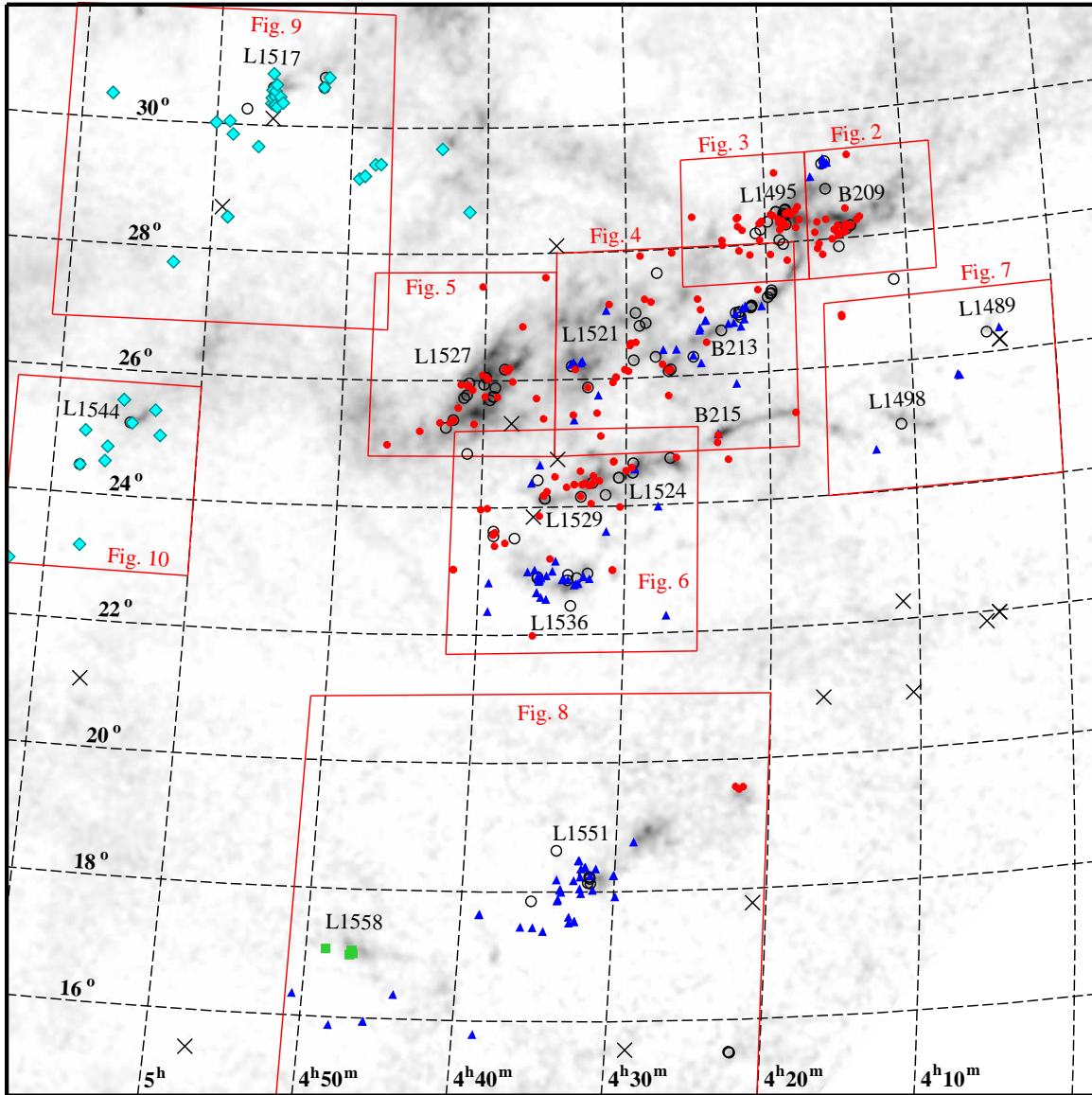


FIG. 1.— Spatial distribution of stars adopted as members of Taurus by Esplin & Luhman (2017). Stars that have parallaxes and proper motions from *Gaia* DR2 are shown with filled symbols (red circles, blue triangles, green squares, cyan diamonds) if they are retained as members in this work or crosses if they are rejected as nonmembers. Members that lack *Gaia* data are plotted with open circles. The filled symbols are assigned based on the kinematic populations in Figures 2–11. The boundaries of the fields encompassed by those figures are marked by the red rectangles. The dark clouds in Taurus are displayed with a map of extinction (gray scale, Dobashi et al. 2005). Designations for some of the most prominent clouds are indicated (Barnard et al. 1927; Lynds 1962).

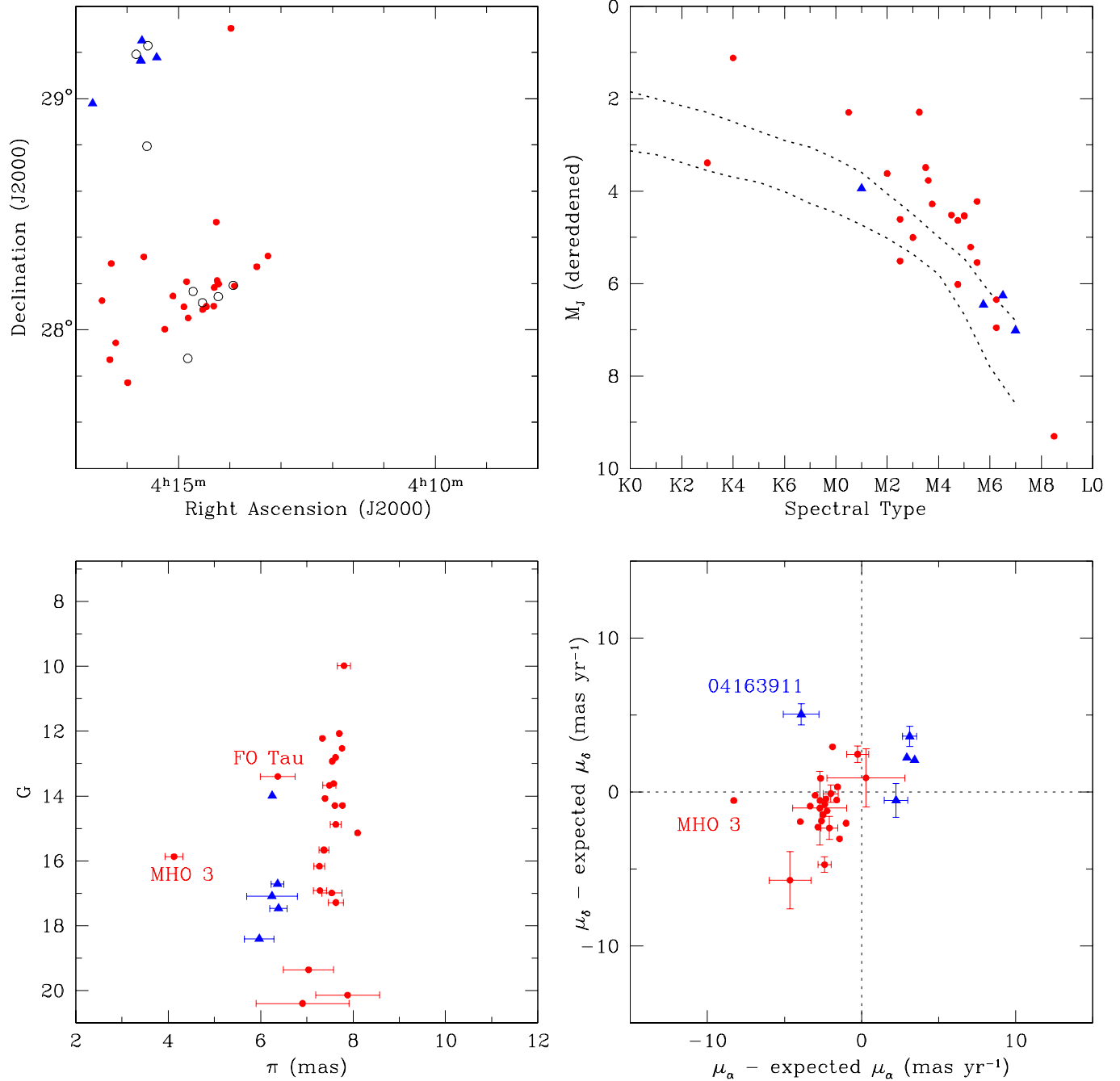


FIG. 2.— Spatial distribution of stars adopted as members of Taurus by Esplin & Luhman (2017) for a field encompassing the B209 cloud (top left). The symbols are the same as in Figure 1. The stars that have parallaxes and proper motions from *Gaia* DR2 are shown in diagrams of extinction-corrected M_J versus spectral type (top right), G versus parallax (bottom left), and proper motion offsets relative to the values expected for the positions and parallaxes of the stars assuming the median space velocity of Taurus members (bottom right). The diagram of M_J versus spectral type includes the median sequences for Taurus and Upper Sco (upper and lower dotted lines). Two stars in B209 with discrepant parallaxes and motions are labeled in the bottom diagrams. They are omitted from M_J versus spectral type. Error bars are omitted in the bottom diagrams when the errors are smaller than the symbols (< 0.1 mas, < 0.5 mas yr^{-1}).

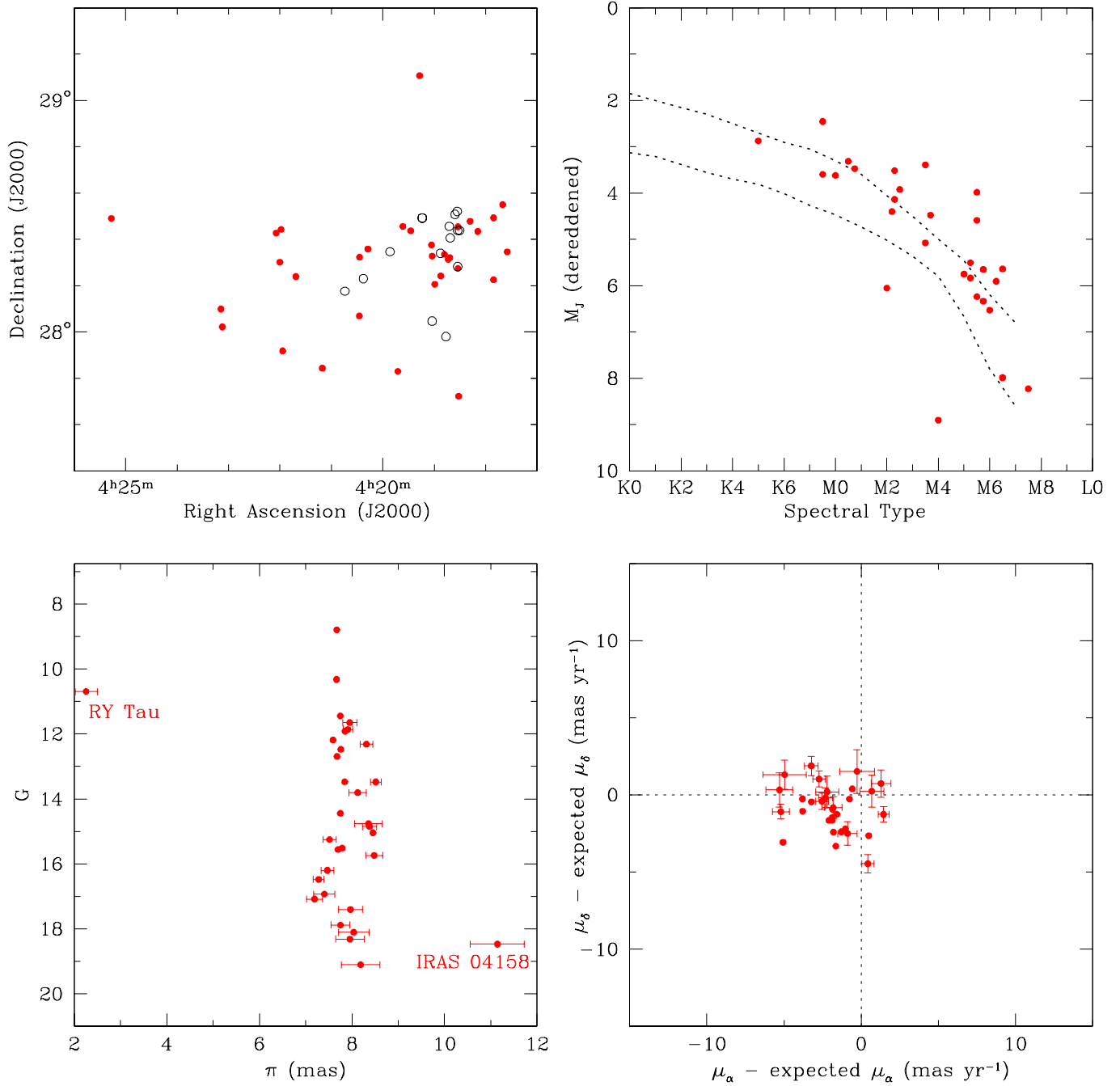


FIG. 3.— Same as Figure 2 for the L1495 cloud.

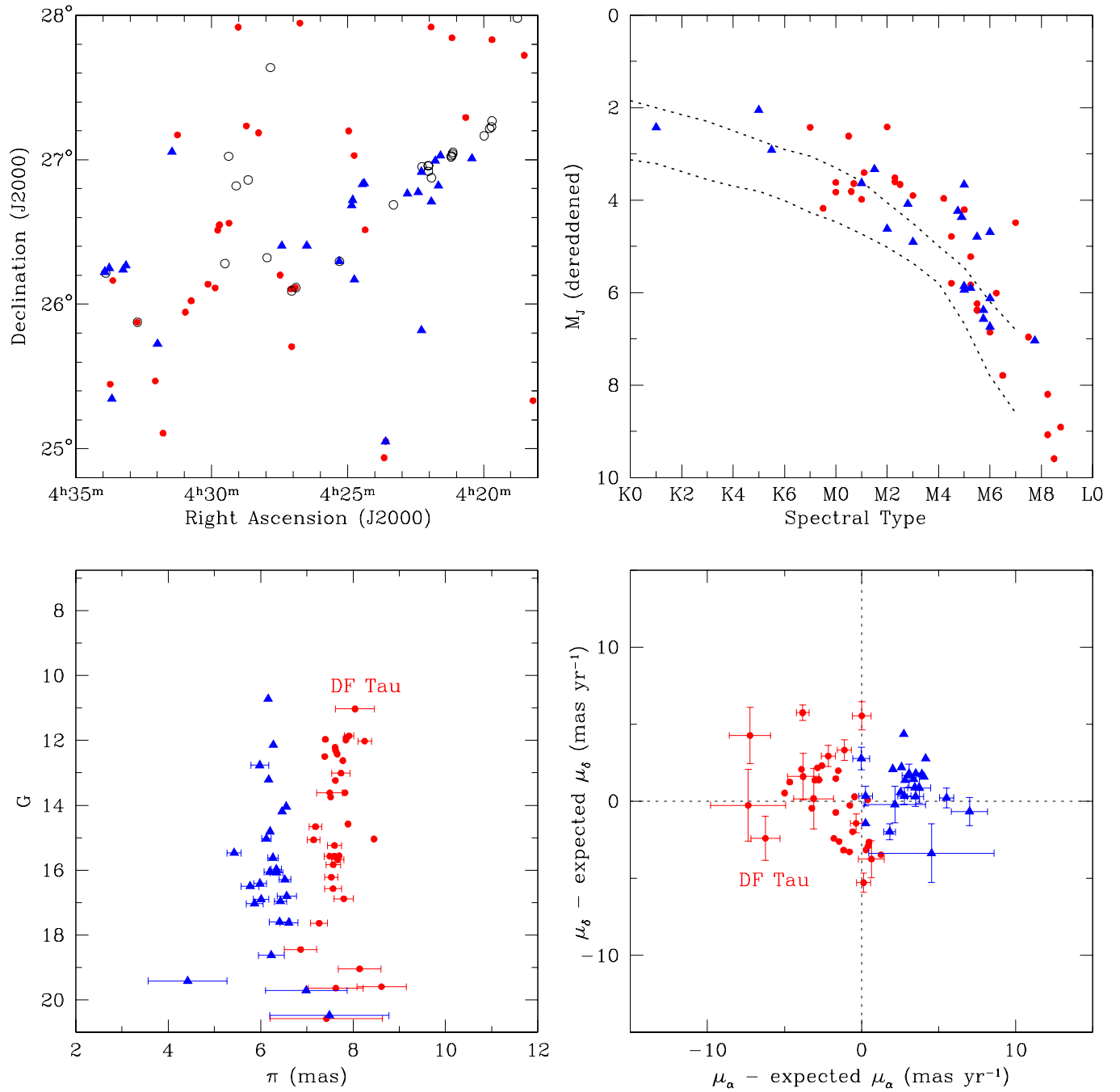


FIG. 4.— Same as Figure 2 for the L1521, B213, and B215 clouds.

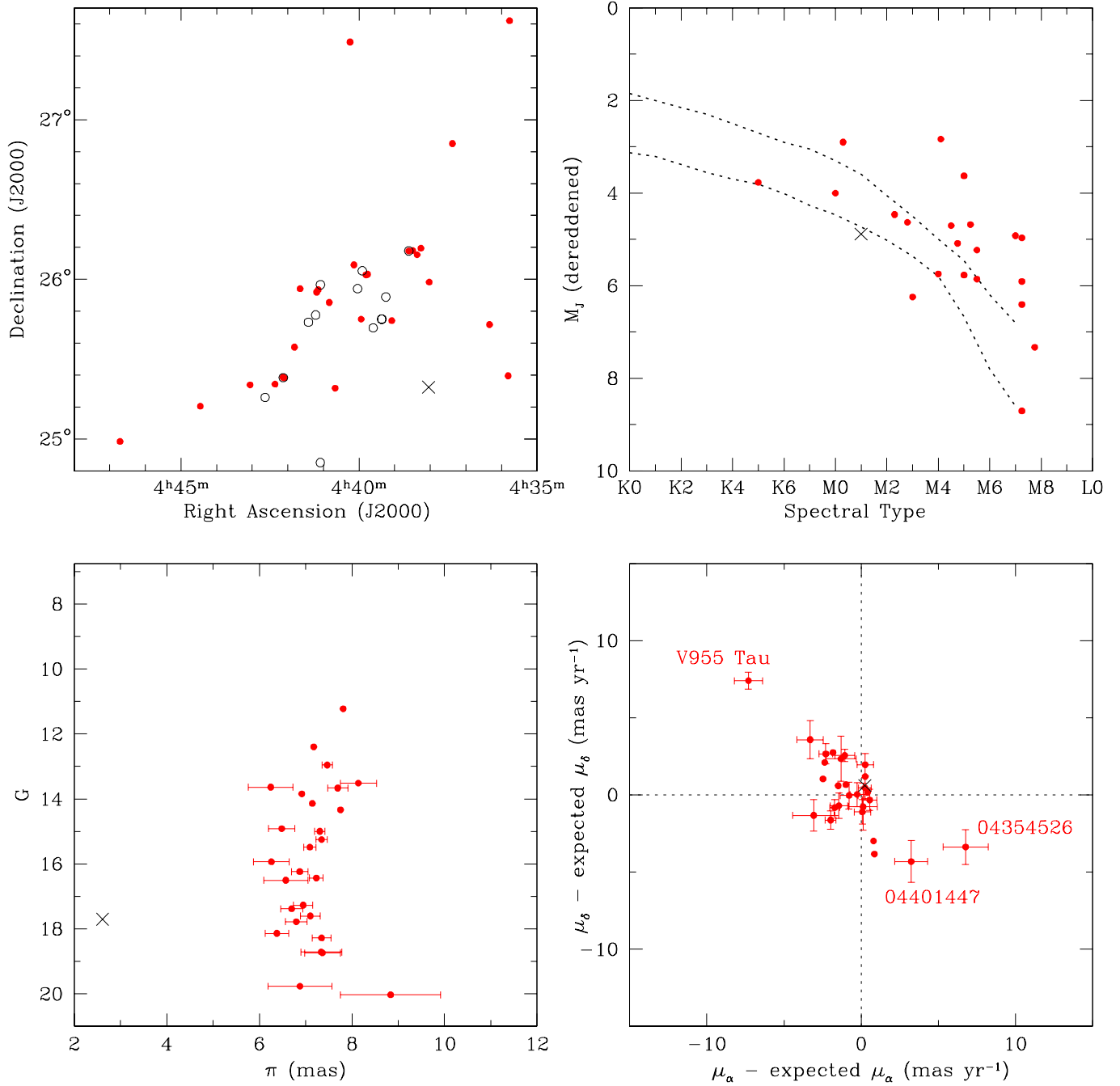


FIG. 5.— Same as Figure 2 for the L1527 cloud.

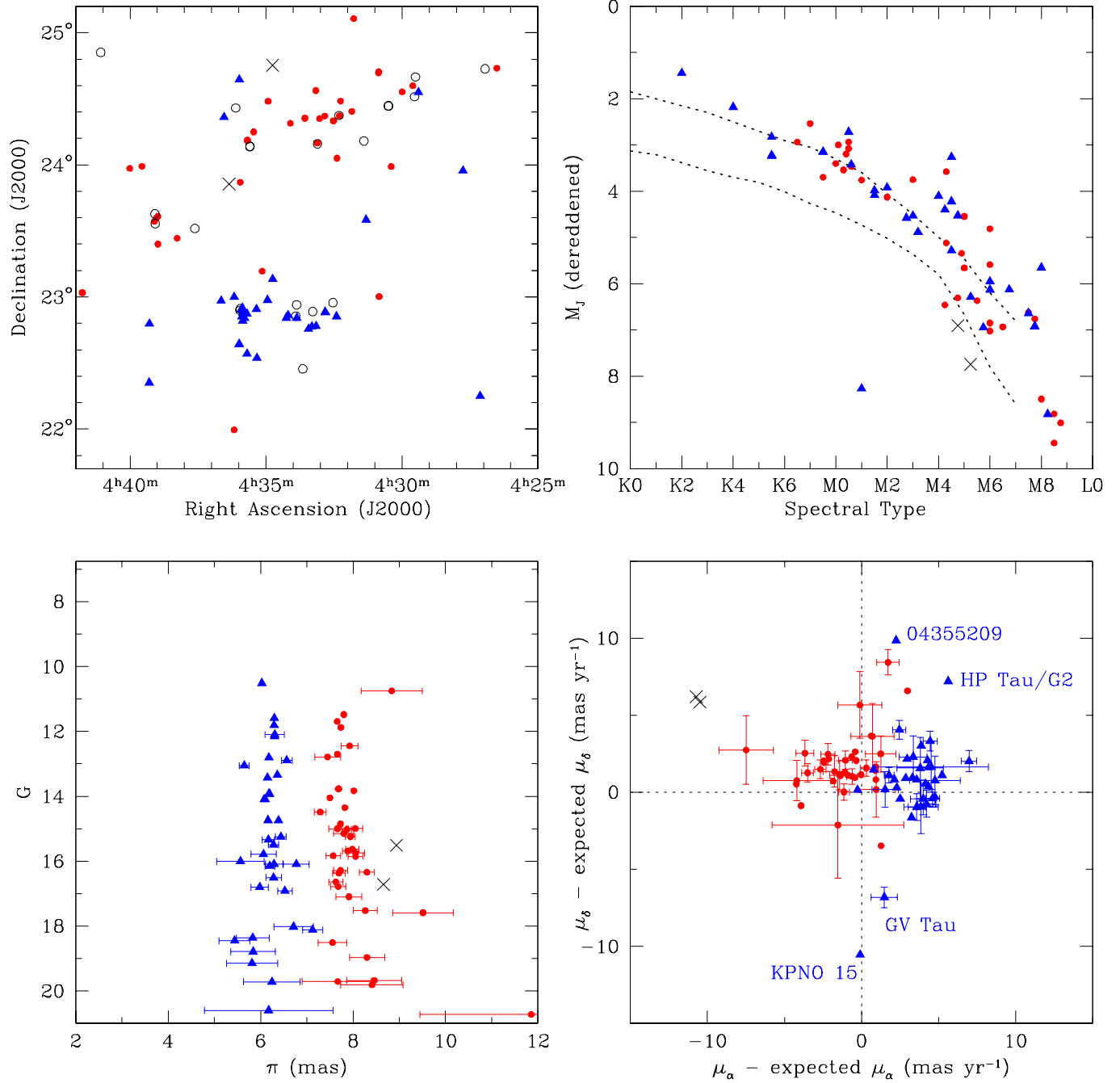


FIG. 6.— Same as Figure 2 for the L1524, L1529, and L1536 clouds.

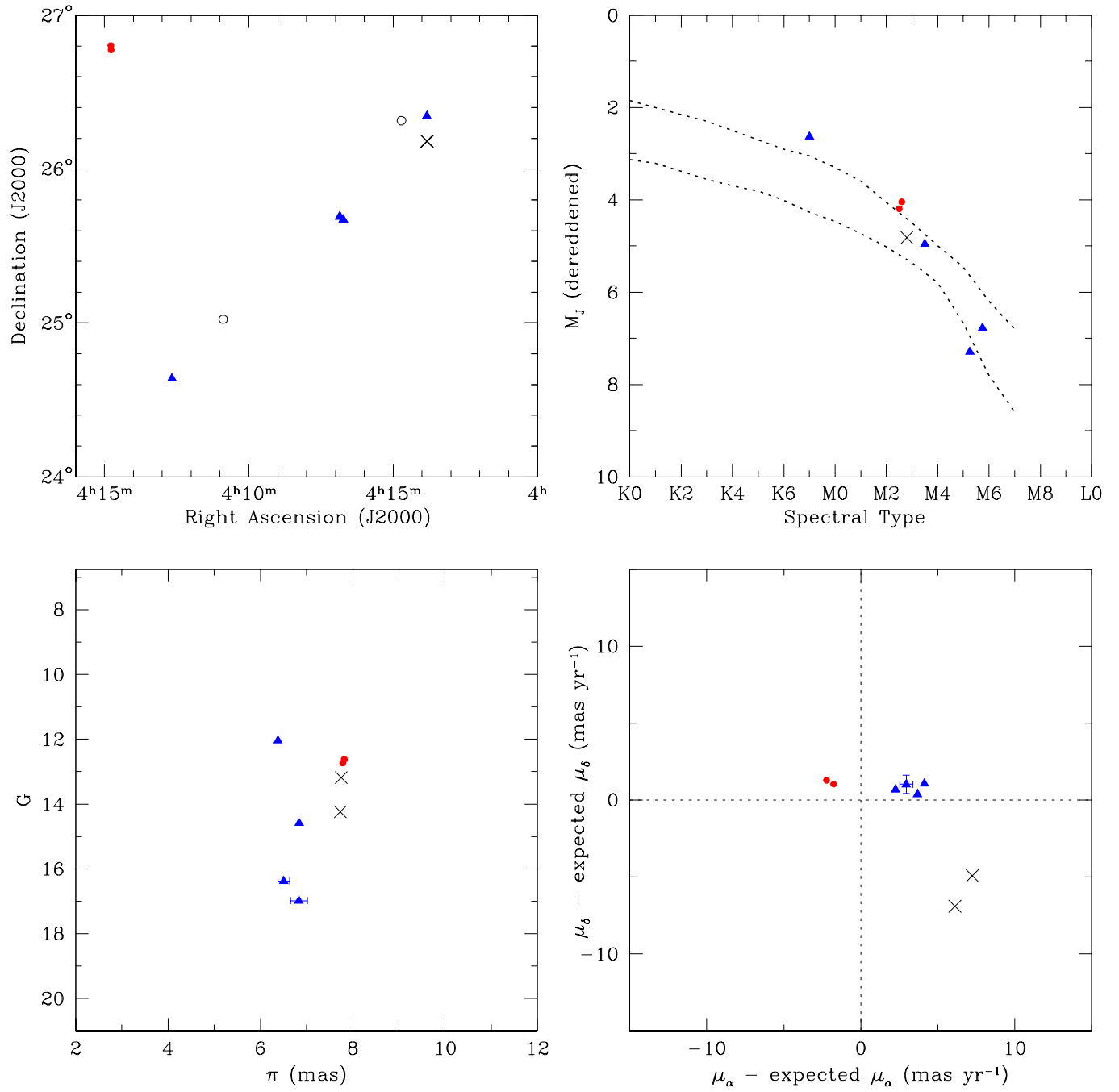


FIG. 7.— Same as Figure 2 for the L1489 and L1498 clouds.

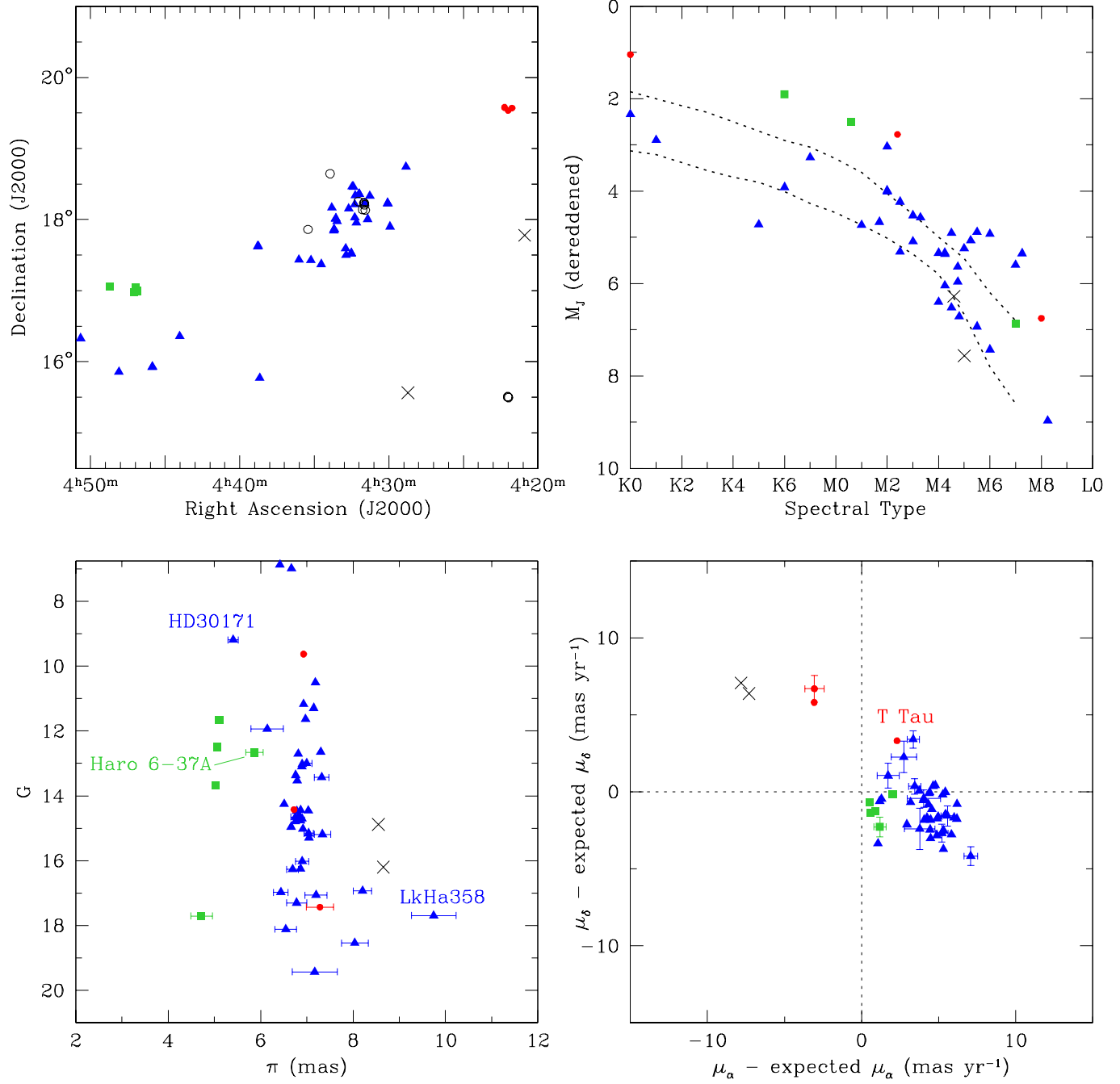


FIG. 8.— Same as Figure 2 for the L1551 and L1558 clouds and the small cloud near T Tau.

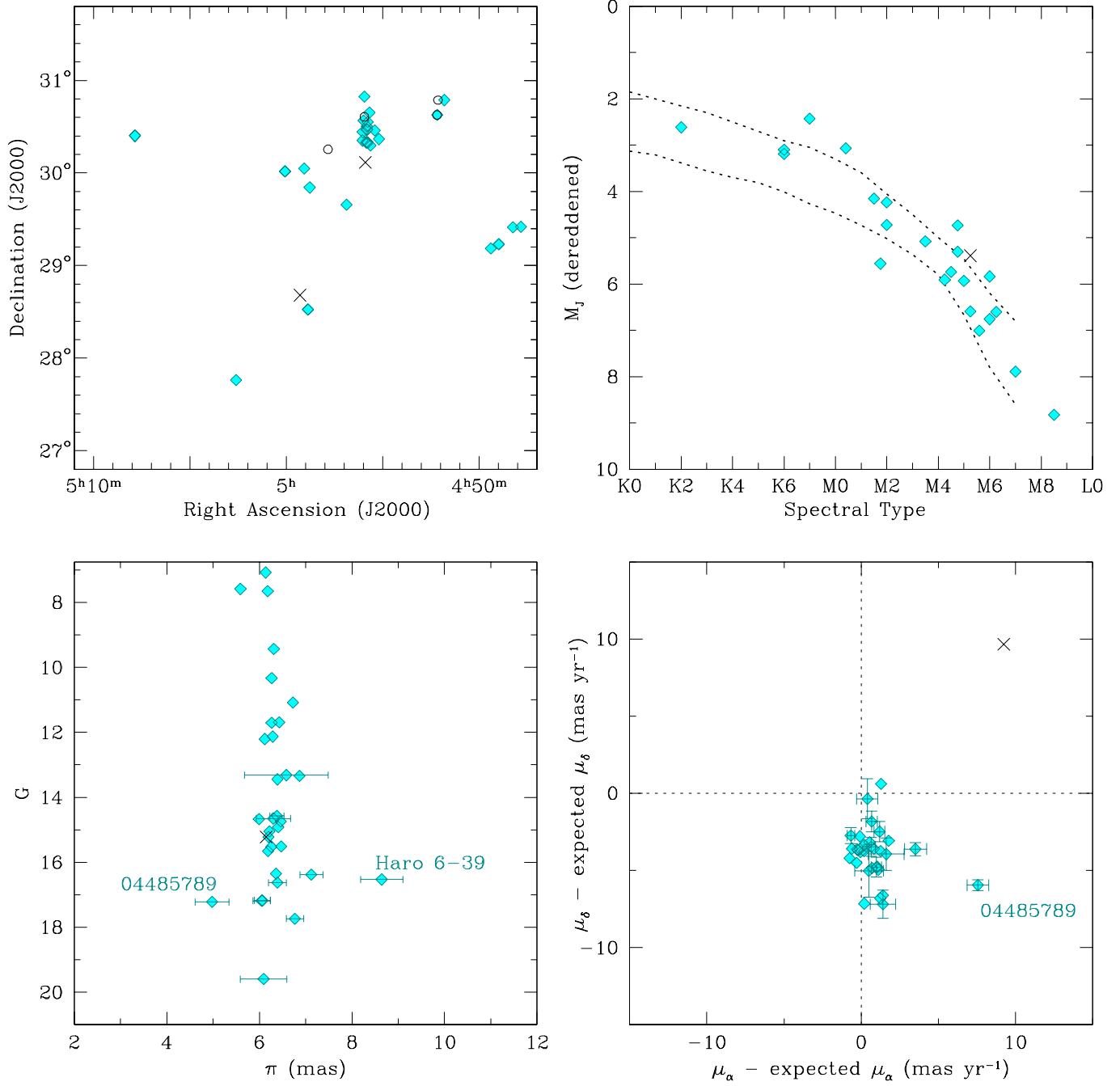


FIG. 9.— Same as Figure 2 for the L1517 cloud.

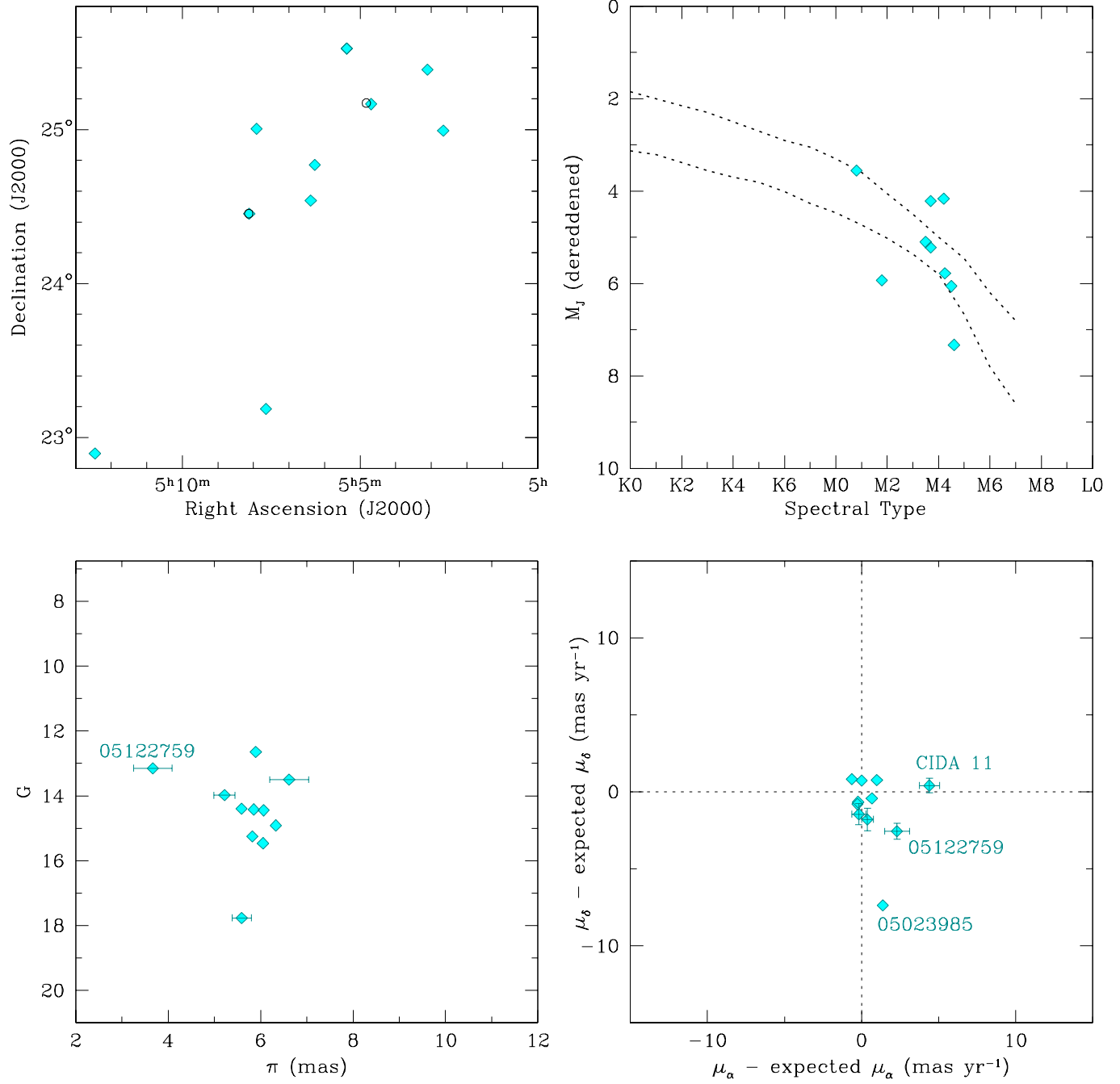


FIG. 10.— Same as Figure 2 for the L1544 cloud.

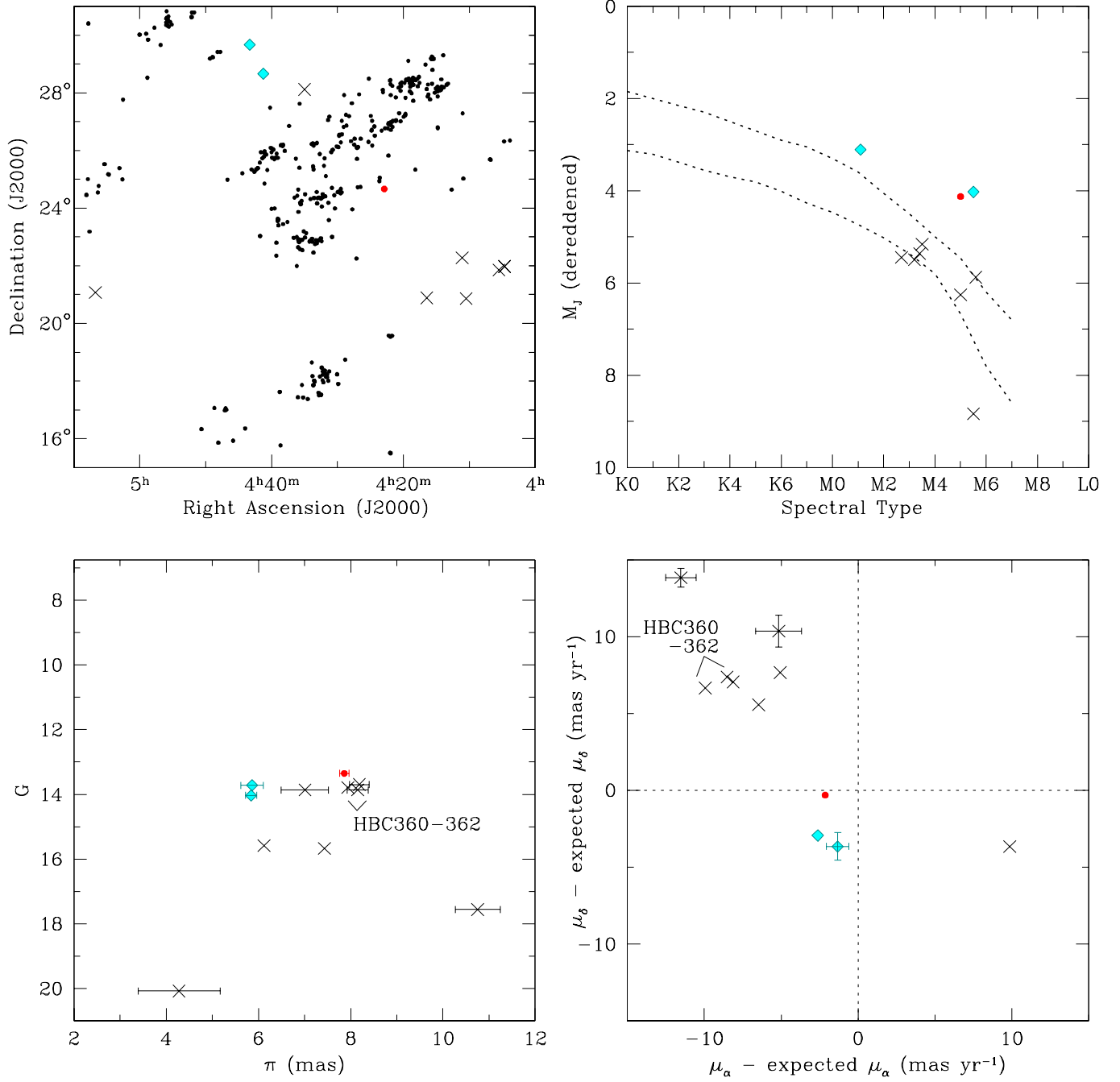


FIG. 11.— Same as Figure 2 for the area outside of the fields in Figures 2–10.

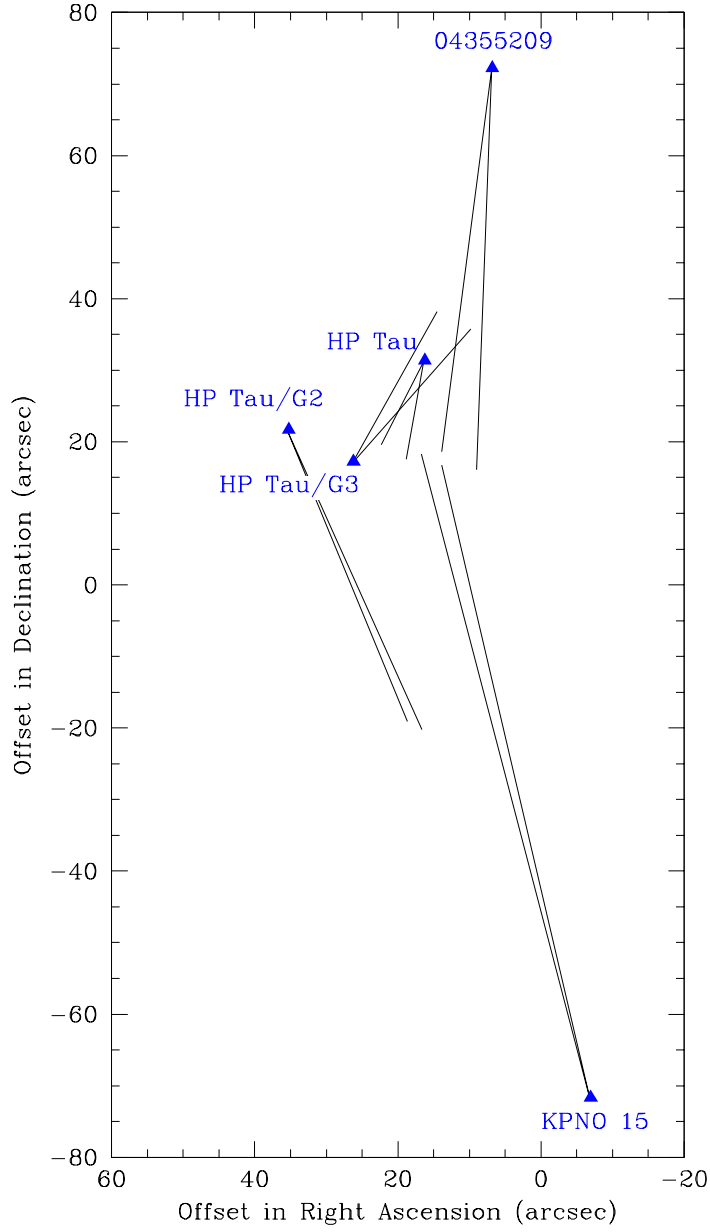


FIG. 12.— Relative positions of two stars in the L1536 cloud with discrepant proper motions (Fig. 6), 2MASS J04355209+2255039 and KPNO 15, and other young stars in their vicinity. Based on proper motions from *Gaia* DR2, those two stars were near the same location ~ 7200 years ago. The allowed paths over that time period are indicated for all stars (1σ , lines), which are computed using the motions relative to the average motion of the stars in this field.

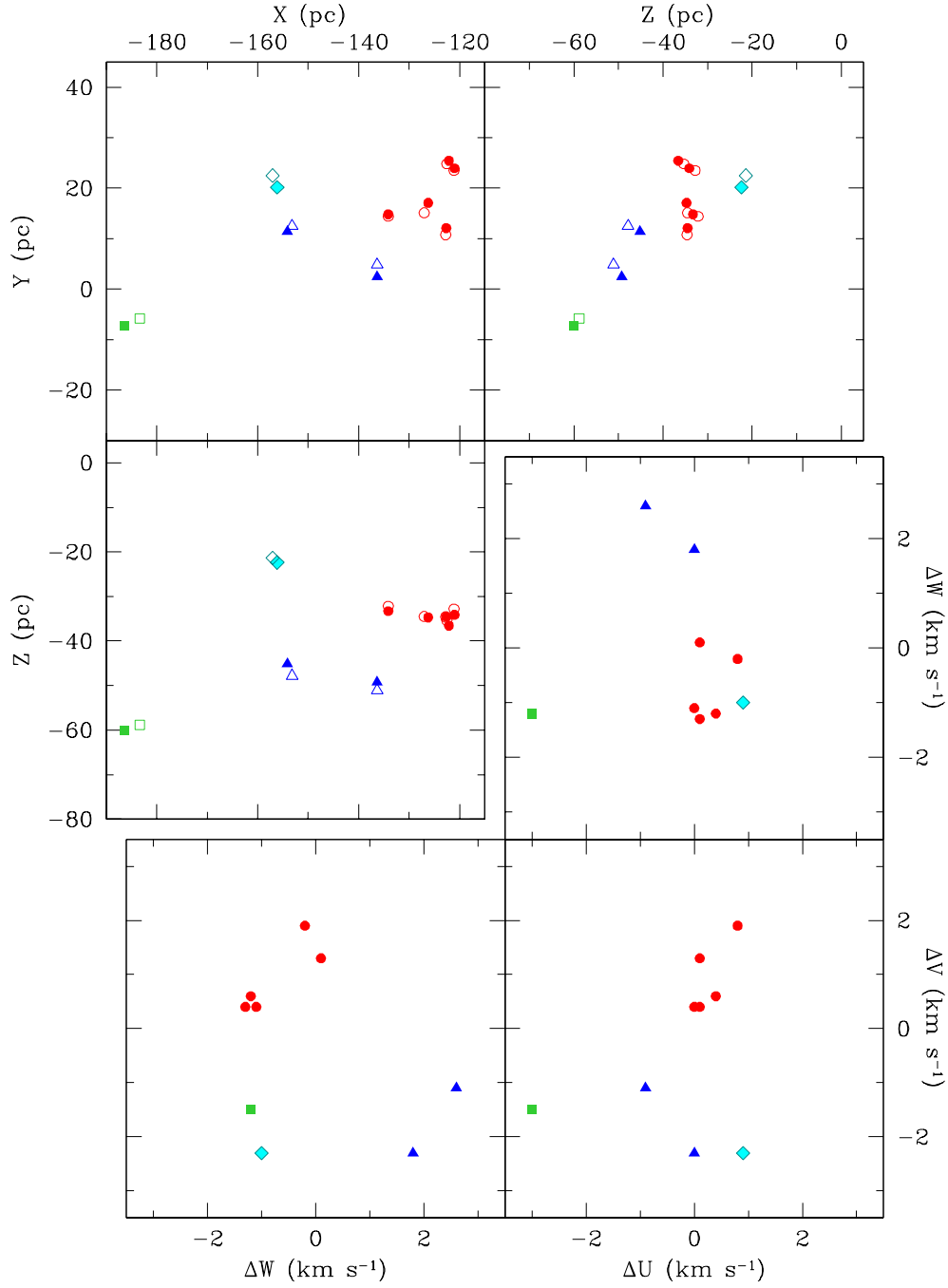


FIG. 13.— Positions and velocity offsets in Galactic Cartesian coordinates for aggregates of stars in Taurus (filled symbols, Table 3). In the diagrams of XYZ , the open symbols represent the projected positions at 1 Myr in the past. The velocity offsets are relative to the median UVW of known Taurus members.

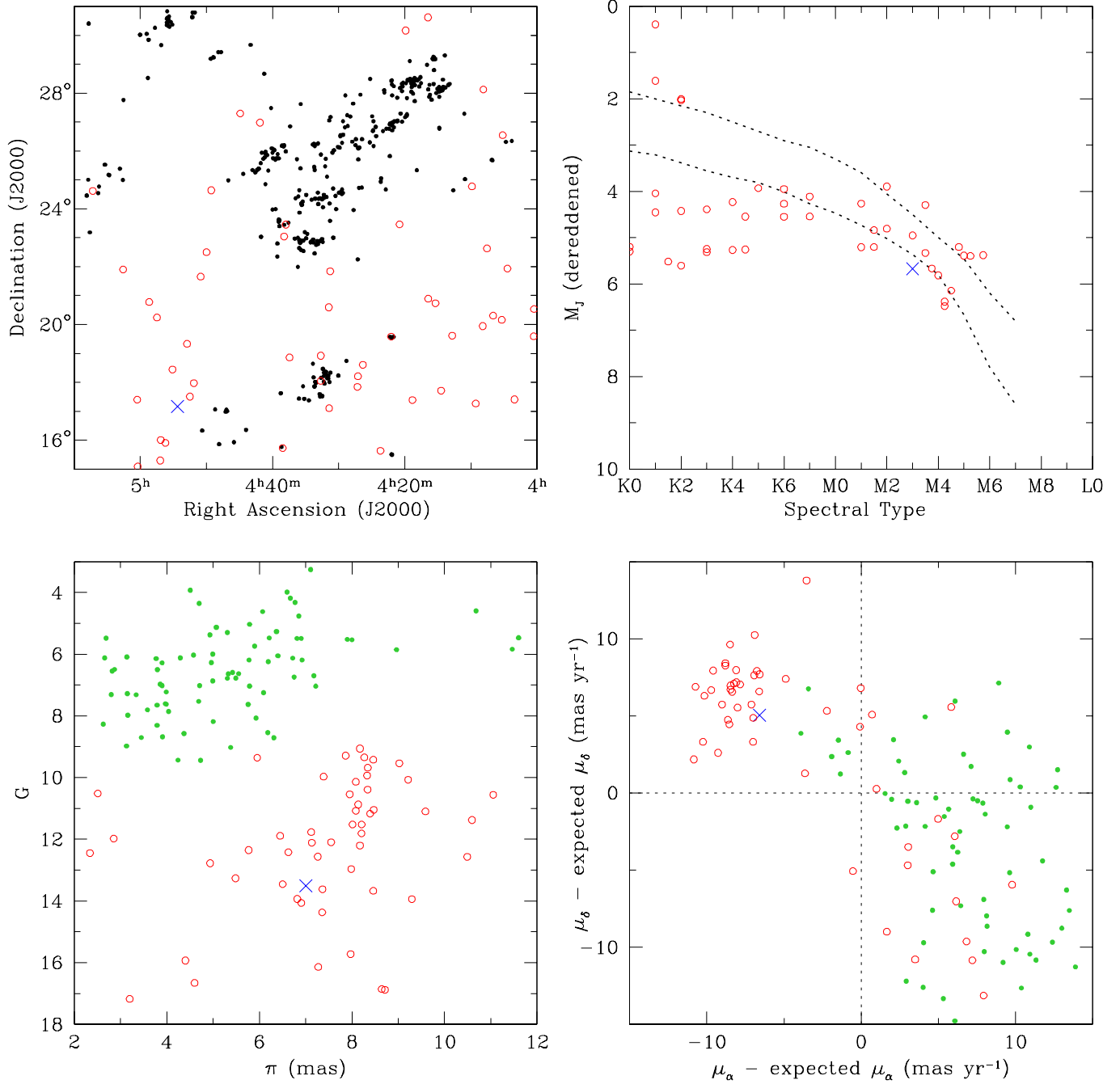


FIG. 14.— Same as Figure 2 for candidate members of Taurus from Kraus et al. (2017) that were not adopted as members by Esplin & Luhman (2017) (red open circles). The map includes the stars compiled by Esplin & Luhman (2017) that are adopted as Taurus members in this work (filled circles; Section 2.3) and the two bottom diagrams include proposed members of Cas-Tau from de Zeeuw et al. (1999) (green filled circles). The young star St34 is also shown in each of the diagrams (blue cross, Hartmann et al. 2005; White & Hillenbrand 2005).

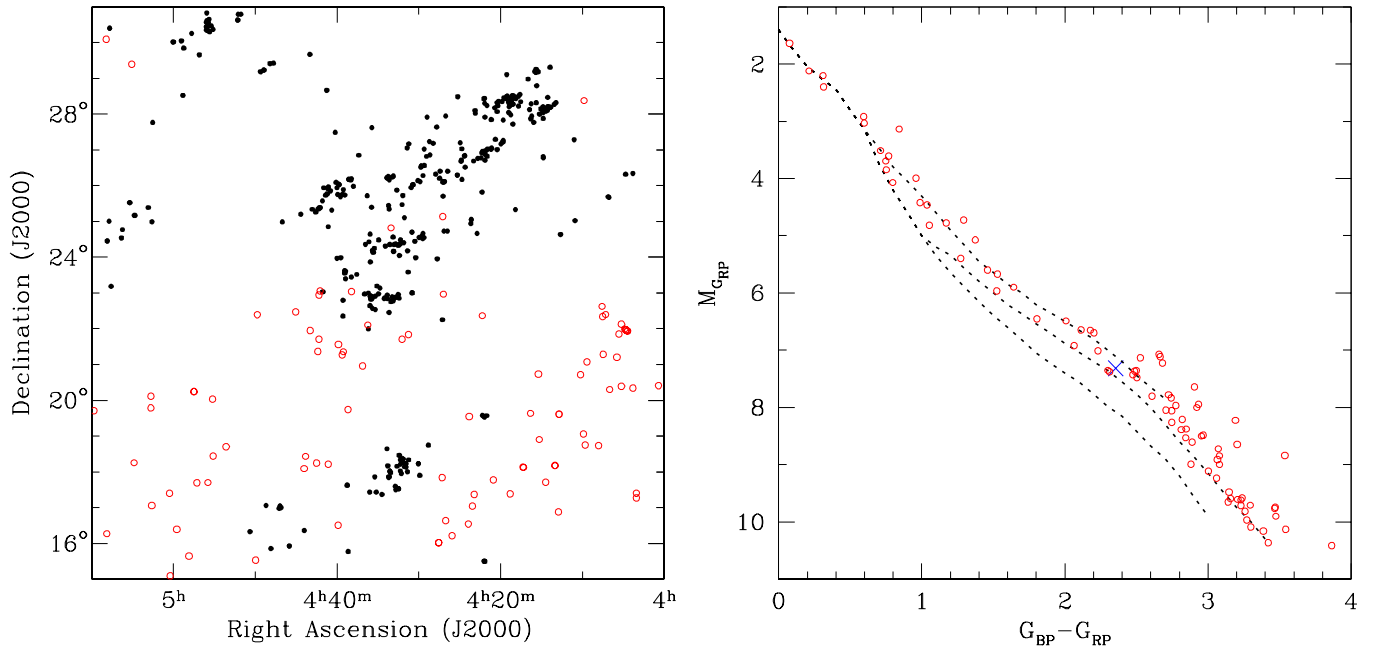


FIG. 15.— Spatial distribution and $M_{G_{RP}}$ versus $G_{BP} - G_{RP}$ for stars towards Taurus that have parallaxes and proper motion offsets similar to those of the clump of candidates from Kraus et al. (2017) at $\pi \sim 8.25$ mas and $(\Delta\mu_{\alpha}, \Delta\mu_{\delta} \sim -8.2, 7.0 \text{ mas yr}^{-1})$ in Figure 14 (red open circles). The map includes the stars compiled by Esplin & Luhman (2017) that are adopted as Taurus members in this work (filled circles; Section 2.3) and the color-magnitude diagram includes fits to the single-star sequences for the β Pic moving group (24 Myr, Bell et al. 2015), the Tuc-Hor association (45 Myr, Bell et al. 2015), and the Pleiades cluster (112 Myr, Dahm 2015) (dotted lines, top to bottom). The young star St34 is also shown in the right diagram (blue cross, Hartmann et al. 2005; White & Hillenbrand 2005).

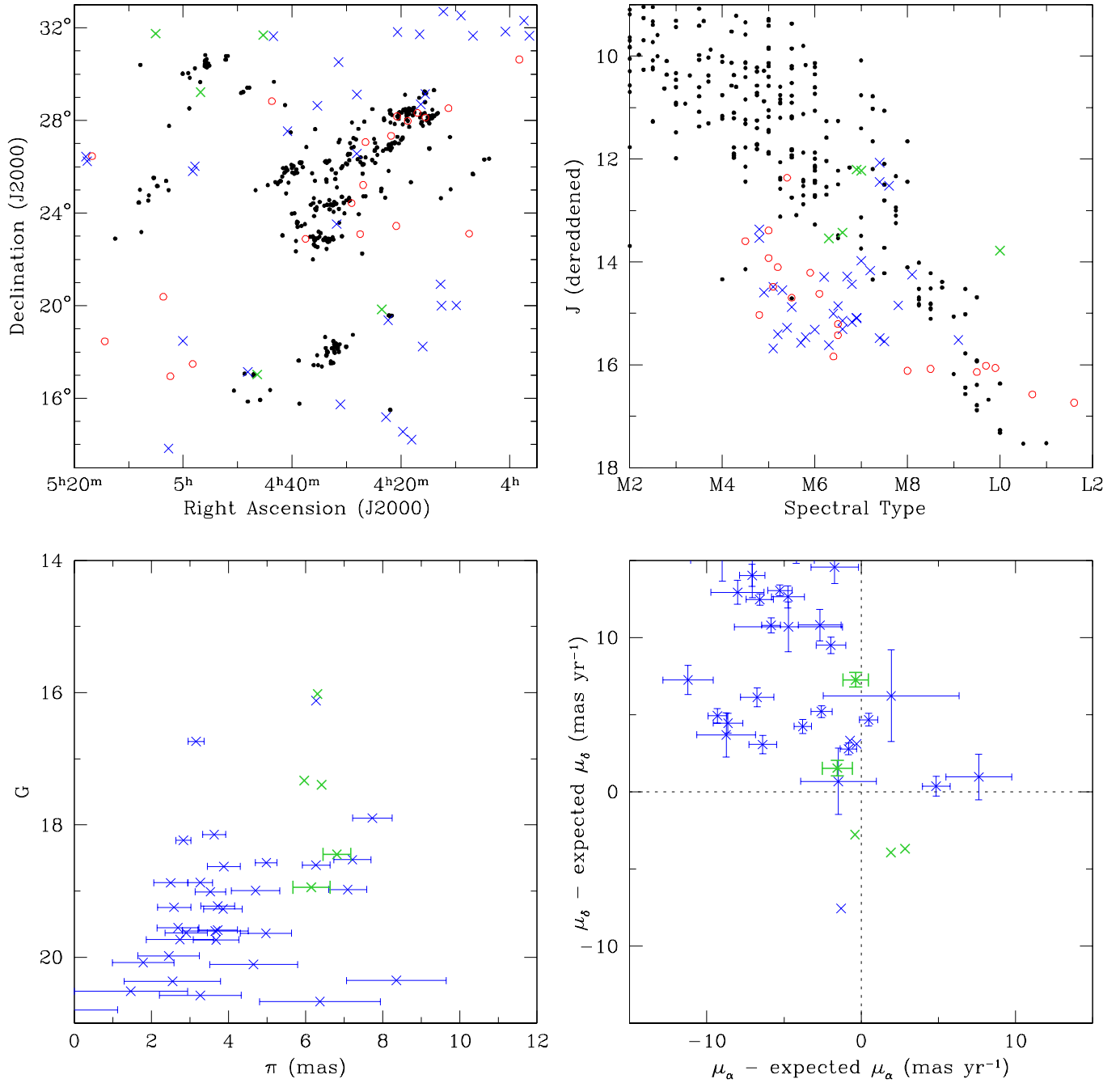


FIG. 16.— Same as Figure 2 for candidate members of Taurus from Zhang et al. (2018) that have parallax measurements from *Gaia* DR2 (blue and green crosses) and those that lack such data (red open circles). The five candidates adopted as members in this work are plotted in green and the other candidates are plotted in blue. The top diagrams include the stars compiled by Esplin & Luhman (2017) that are adopted as Taurus members in this work (filled circles; Section 2.3).

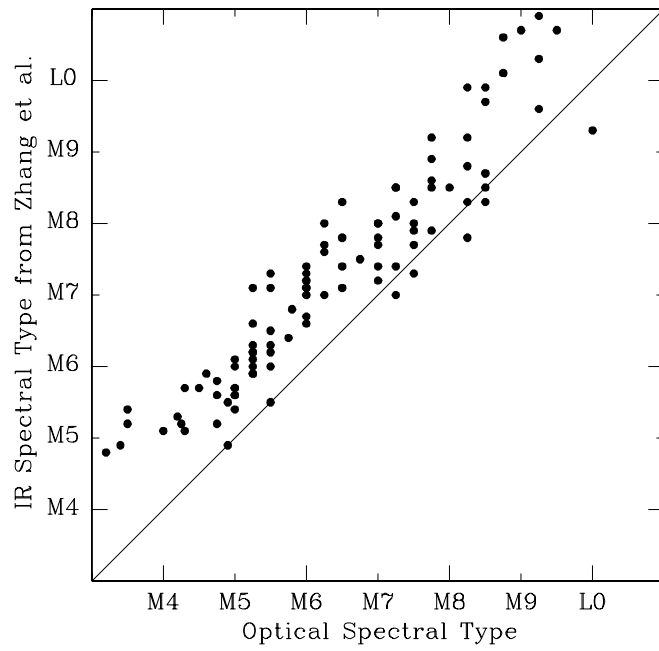


FIG. 17.— Near-IR spectral types from Zhang et al. (2018) versus optical spectral types from previous studies (see Section 3.2) for known members of Taurus that were classified in the former study.

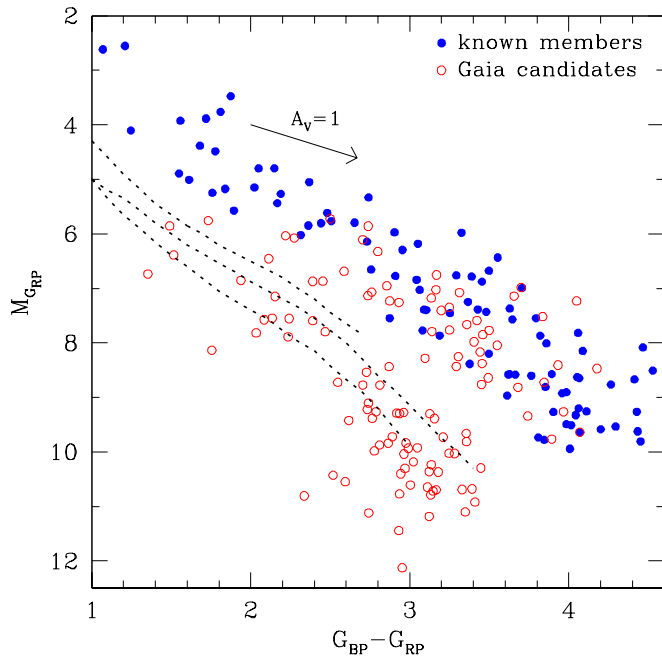


FIG. 18.— $M_{G_{\text{RP}}}$ versus $G_{\text{BP}} - G_{\text{RP}}$ for known members of Taurus that lack disks (blue filled circles) and candidate members in the nine fields in Figure 1 that were selected from *Gaia* DR2 to have parallaxes and proper motion offsets similar to those of the Taurus populations in those fields (red open circles). I have included fits to the single-star sequences for the β Pic moving group (24 Myr, Bell et al. 2015), the Tuc-Hor association (45 Myr, Bell et al. 2015), and the Pleiades cluster (112 Myr, Dahm 2015) (dotted lines, top to bottom).

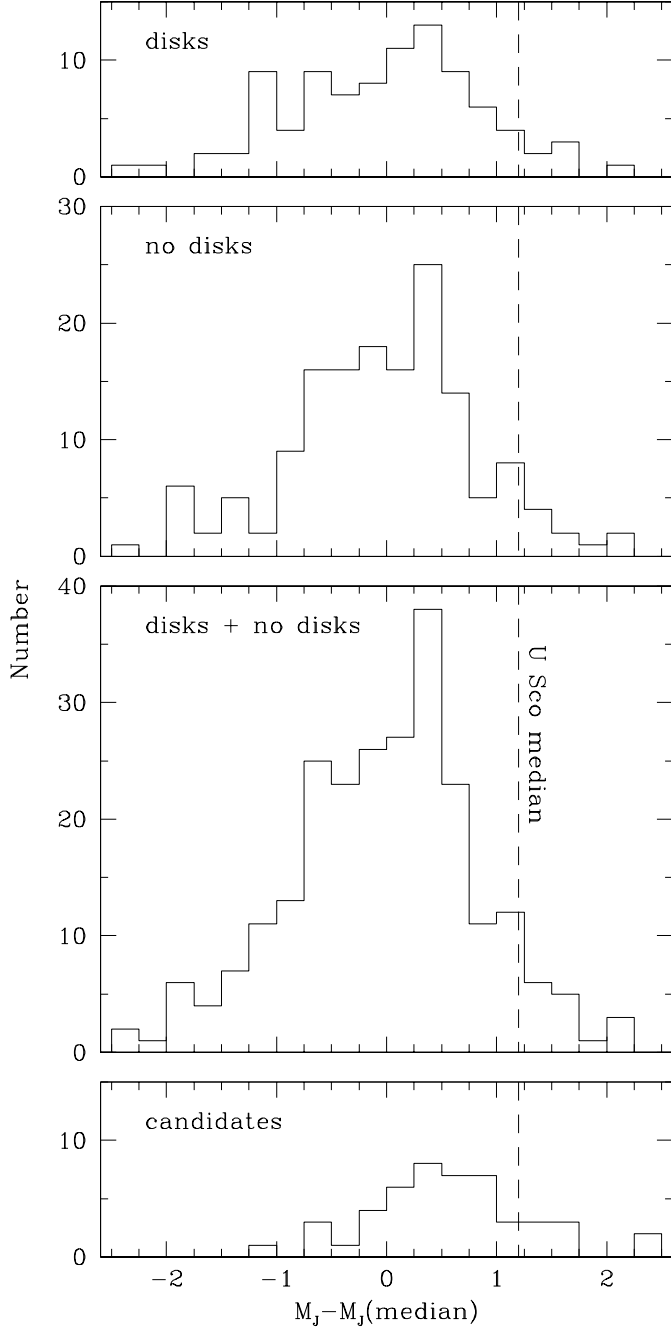


FIG. 19.— Distributions of offsets of extinction-corrected M_J from the median sequence for disk-bearing and diskless members of Taurus at K0–M7. The distribution for the candidate members above the Tuc-Hor sequence in Figure 18 is also shown (Table 6). The offset of the median sequence for Upper Sco is indicated (dashed line), which has an age of 11 Myr (Pecaut et al. 2012).

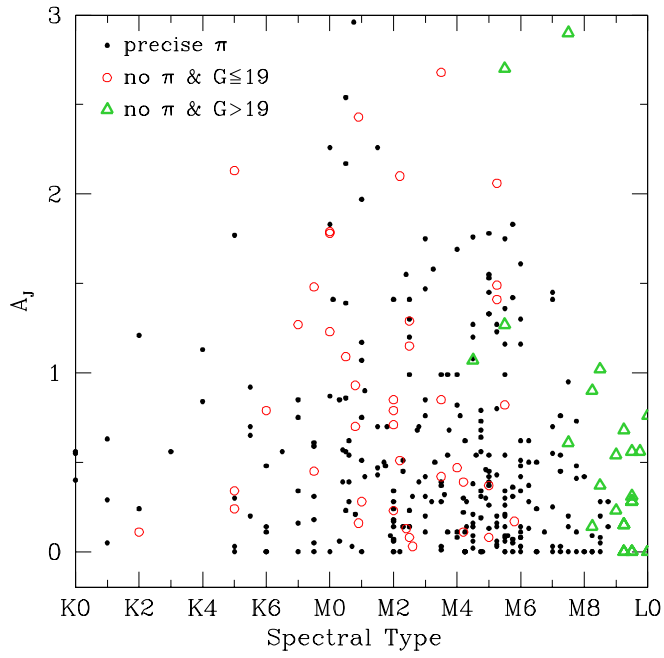


FIG. 20.— A_J versus spectral type for K0–L0 members of Taurus, which are labeled according to whether they have precise parallax measurements from *Gaia* DR2 ($\pi/\sigma_\pi \geq 10$, filled circles) or lack precise parallaxes and have $G \leq 19$ (red open circles) or $G > 19$ (green triangles). The fraction of stars in DR2 that have parallaxes is high down to $G \sim 19$. The Taurus members at $G \leq 19$ without precise parallaxes have erroneous astrometry because of extended emission or close companions.

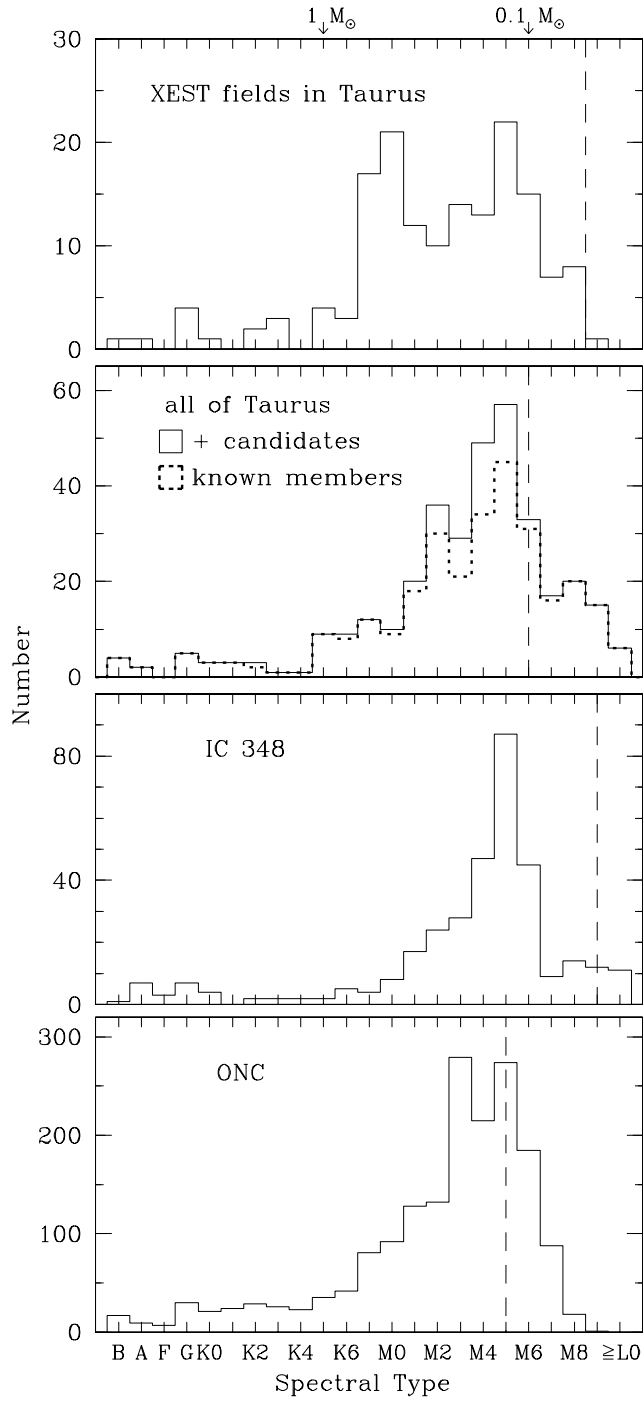


FIG. 21.— Distributions of spectral types for the XEST fields in Taurus as measured by Luhman et al. (2009), the entirety of Taurus for $A_J < 1$ (this work), IC 348 for $A_J < 1.5$ (Luhman et al. 2016), and the ONC (Da Rio et al. 2012; Hillenbrand et al. 2013). The dashed lines indicate the completeness limits of these samples and the arrows mark the spectral types that correspond to masses of 0.1 and $1 M_{\odot}$ for ages of a few Myr according to evolutionary models (e.g., Baraffe et al. 1998).